ACS OMEGA

http://pubs.acs.org/journal/acsodf

Article

Thermochemical Properties and Growth Mechanism of the Ag-Doped Germanium Clusters, $AgGe_n^{\lambda}$ with $n = 1-13$ and $\lambda = -1$, 0, and +1

Bin Liu and Jucai Yang*

Cite This: *ACS Omega* 2021, 6, 9813−9827

Read Online

ACCESS | Metrics & More | Article Recommendations

ABSTRACT: A systematic investigation of the silver-doped germanium clusters $AgGe_n$ with $n = 1-13$ in the neutral, anionic, and cationic states is performed using the unbiased global search technique combined with a double-density functional scheme. The lowest-energy minima of the clusters are identified based on calculated energies and measured photoelectron spectra (PES). Total atomization energies and thermochemical properties such as electron affinity (EA), ionization potential (IP), binding energy, hardness, and highest occupied molecular orbital-lowest unoccupied molecular orbital (HOMO-LUMO) gap are obtained and compared with those of pure germanium clusters. For neutral and anionic clusters, although the most stable structures are inconsistent when $n = 7-10$, their structure patterns have an exohedral structure except for $n = 12$, which is a highly symmetrical endohedral configuration. For the cationic state, the most stable structures are attaching structures (in which an Ag atom is adsorbed on the Ge_n cluster or a Ge atom is adsorbed on the $AgGe_{n-1}$ cluster) at $n = 1-12$, and when $n = 13$, the cage configuration is formed. The analyses of binding energy indicate that doping of an Ag atom into the neutral and charged Ge_n clusters decreases their stability. The theoretical EAs of $AgGe_n$ clusters agree with the experimental values. The IP of neutral Ge_n clusters is decreasing when doped with an Ag atom. The chemical activity of $AgGe_n$ is analyzed through HOMO-LUMO gaps and hardness, and the variant trend of both versus cluster size is slightly different. The accuracy of the theoretical analyses in this paper is demonstrated successfully by the agreement between simulated and experimental results such as PES, IP, EA, and binding energy.

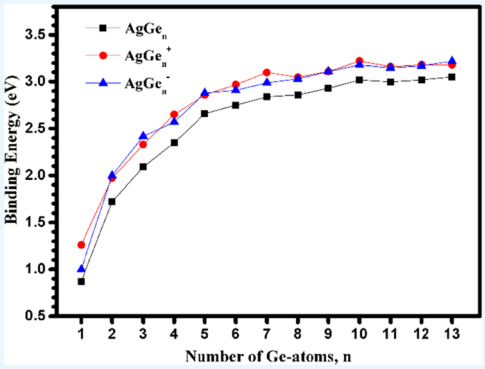

1. INTRODUCTION

With the rapid development of nanotechnology, the research on the geometric configuration and electronic properties of clusters has become more important because clusters play a pivotal role in the transition from the molecule to the condensed phase, especially for semiconductor clusters owing to their interesting chemical structures and bonding motifs, as well as their importance in the microelectronics industry.[1−15] However, pure semiconductor clusters such as germanium clusters are unstable because they show only sp^3 bonding characteristics.[16−20] Recently, a lot of experimental and theoretical research studies have elucidated that introducing a transition metal atom into germanium clusters can not only heighten their stability, but also deeply affect their electron properties.[21−50] Studying the structure and growth model of different transition metal (TM)-doped germanium clusters can not only find a stable cage configuration that can be used as a nanomaterial structure, but also lay a foundation for their special physical and chemical properties. To understand how these attractive physical−chemical properties attribute to the doped clusters, it is important to gain the comprehensive knowledge of the ground state and lower-lying electronic and geometric configurations of charged and neutral TM-doped Ge clusters. Therefore, Nakajima and his colleagues have first explored the electronic and geometric configurations of $TMGe_n$ (TM = Sc, Y, Ti, Zr, Hf, V, Nb, Ta, and Lu; $n = 8-20$) clusters by means of dissecting their mass spectra, photoelectron spectra (PES), and reactivities to H_2O adsorption.[21] Then Zheng and co-workers reported the electron affinities (EAs) and the electronic structures of TM_xGe_n (TM = Ag, Au, Ti, V, Co, Fe, and Cr; $x \leq 2$; $n \leq 14$) through recording and analyzing their PES.[22−31] Prompted by the experimental observations, some theoretical calculations and simulations of TM-doped germanium clusters have been carried out. For instance, the geometries and electronic

Received: January 27, 2021
Accepted: March 24, 2021
Published: March 31, 2021

structures of small sized clusters $TiGe_2^{-/0}$, $VGe_3^{-/0}$, $CrGe_n^{0/+}$ (n = 1−5), $NbGe_n^{-/0/+}$ (n = 1−3), and $VGe_n^{-/0}$ (n = 5−7) have been investigated through multiconfigurational methods.[32−36] Wang et al. explored the structural evolution, stability, and electronic properties of $MnGe_n$ (n = 2−15) by means of the Perdew−Burke−Ernzerhof (PBE) functional and found that the threshold size for the formation of caged $MnGe_n$ and the sealed Mn-encapsulated Ge_n motif is n = 9 and 10, respectively.[37] Kapila et al. investigated the ground-state structures and magnetic moments of $CrGe_n$ (n = 1−13) using the PBE functional and found that the magnetic moment in their ground-state structure is either 4 μB or 6 μB.[38] Bandyopadhyay and co-workers studied the evolution of configuration, electronic properties, and stability of positively charged and neutral $TMGe_n$ clusters (TM = Mo, Nb, Ni, Sc, Ti, V, Zr, Hf, Cu, and Au; $n \leq 20$) using B3LYP or B3PW91 density functional theory (DFT) and presented that the size of the smallest TM-encapsulated into Ge_n configurations was n = 8 for Nb, n = 9 for Zr, Ti, Hf, and Cu, n = 10 for Mo, and n = 11 for Au atoms.[39−45] Rabilloud and co-workers explored the configurations, electronic properties, and magnetic moments of $TMGe_n$ (TM = V, Nb, Ta, Pd, Pt, Cu, Ag, and Au; $n \leq 21$) species using the PBE functional and reported that the smallest size of the TM-encapsulated to Ge_n cage was n = 10 for Cu and V and n = 12 for Au and Ag.[17−20] It is stated that the smallest size of the $CuGe_n$ cluster evaluated using the PBE functional differs from that evaluated using the B3PW91 functional. For negatively charged ions, Borshch et al. evaluated the ground-state structures of $TMGe_n^-$ (TM = Sc, Zr, Hf, Nb, and Ta; $n \leq$ 20), simulated their PES by employing the B3LYP functional, and found that the smallest size of $TM@Ge_n^-$ was n = 12 for Zr, Nb, Hf, and Ta, but n = 13 for Sc atoms.[46−50] Kumar and co-workers studied the equilibrium geometry and electronic structure of $ZrGe_n^{-/0}$ (n = 1−21) with the PW91 functional, compared their simulated PES with experimental ones, and found that in some cases a higher energy configuration of $ZrGe_n^-$ species may be present in experiments, but the neutral of such an anion is often the lowest energy isomer.[51] Trivedi et al. explored the structural stability and electronic and vibrational properties of M@Xn (M = Ag, Au, Co, Pd, Tc, and Zr; X = Ge and Si; n = 10, 12, and 14) with the B3LYP scheme.[52,53] Despite performing many theoretical studies on the structural evolution and electronic properties of TM-doped germanium clusters,[17−20,32−54] this work, according to our knowledge, is the first systematic study of charged Ag-doped germanium clusters. Moreover, the lowest-energy structures for neutral $AgGe_n$ with n = 7, 9, 10, 11, and 13 calculated in this study differ from those reported previously.[19] In this work, an artificial bee colony algorithm for cluster global optimization (ABCluster)[55−57] combined with a double-hybrid density functional is employed for the structure optimization of charged and neutral Ag-doped germanium clusters, $AgGe_n^{\lambda}$ (n = 1−13; λ = −1, 0, and +1), with the goal of probing the structural evolution and stability, evaluating thermochemical parameters and electronic properties, and comparing them with charged and neutral pure Ge clusters Ge_{n+1}^{λ} (n = 1−13; λ = −1, 0, and +1), respectively.

2. COMPUTATIONAL METHODS

The initial isomers for $AgGe_n^{\lambda}$ (n = 1−13; λ = −1, 0, and +1) species were based on the ABCluster[55−57] combined with the Gaussian 09 codes.[58] More than 400 isomers for each cluster were first optimized using the PBE0 functional[59] with the effective core potential LanL2DZ basis set[60] for Ge atoms and the cc-pVDZ-PP basis set[61] for Ag atoms. Then, the lower-lying configurations were selected and reoptimized via the PBE0 functional and cc-pVTZ-PP basis set[61,62] for Ge and Ag atoms. Harmonic vibrational frequency calculations were carried out at the same level to guarantee that the configurations were true local minimal structures on the potential energy surface. After completing the initial geometrical optimization using the PBE0/cc-pVTZ-PP scheme, once again, we selected the lower-lying candidates and reoptimized them at the mPW2PLYP/cc-pVTZ-PP level[63] without frequency calculations. Finally, single-point energy calculations were carried out using the mPW2PLYP functional in conjunction with the aug-cc-pVTZ-PP basis set[61] for Ag atoms and the all-electron aug-cc-pVTZ basis set[64] for Ge atoms to further refine the energy. At the mPW2PLYP/aug-cc-pVTZ-PP//mPW2PLYP/cc-pVTZ-PP level, the single-point energy calculations were also performed for comparison.

To check the quality of our used scheme, test calculations were previously performed using the ROCCSD(T) method for $ScSi_n^{0/-}$ (n = 4−9) clusters and compared with several DFT functionals (PBE, B3LYP, TPSSh, wB97X, and mPW2PLYP).[65] The results revealed that (i) only the ground-state structure of $ScSi_n^{0/-}$ (n = 4−9) clusters predicted by the mPW2PLYP functional is consistent with that calculated by the ROCCSD(T) scheme and (ii) the evaluated vertical detachment energy (VDE) by ROCCSD(T) and mPW2PLYP schemes is in good agreement with the experimental data. The mean absolute deviations of VDE from the experiment for $ScSi_n$ (n = 4−7 and 9) are by 0.08, 0.09, 0.13, 0.19, and 0.21 eV at the ROCCSD(T), mPW2PLYP, B3LYP, TPSSh, and PBE levels, respectively. Further to check the quality of the mPW2PLYP scheme, the bond length and frequency of Ge_2 and AgGe dimers were measured using several DFT functionals (PBE0, TPSSh, B3LYP, and mPW2PLYP) combined with cc-pVTZ-PP basis sets for Ge and Ag atoms and are listed in Table 1. The bond

Table 1. Bond Length (Å) and Frequency (cm^{-1}) of Ge_2 and AgGe Dimers Calculated by Different Functionals Combined with the cc-pVTZ-PP Basis Set for Ge and Ag Atoms

	Ge_2		AgGe	
	bond length	frequency	bond length	frequency
PBE0	2.38	290.72	2.45	203.34
TPSSh	2.39	280.94	2.44	210.83
mPW2PLYP	2.38	286.29	2.45	201.89
B3LYP	2.41	275.20	2.47	196.41
Expt.	2.368[a]	287.9[a]	2.54[b]	

[a]ref 15. [b]ref 66.

length of Ge_2 and AgGe calculated using the mPW2PLYP scheme is 2.38 and 2.45 Å, which agrees with the experimental values of 2.368[15] and 2.54 Å,[66] respectively. The frequency of Ge_2 evaluated using the mPW2PLYP scheme is 286.3 cm^{-1}, which is in excellent agreement with the experimental value of 287.9 cm^{-1}.[15] The bond distance of 2.34 Å for Au-Ge predicted by the mPW2PLYP scheme is in good agreement with the experimental value of 2.38 Å.[67] Furthermore, the ABCluster's developers presented many successful examples of ABCluster in a recent article.[57] It is proven to be a successful technique for searching the global minimal structure of atomic and

https://doi.org/10.1021/acsomega.1c00501
ACS Omega 2021, 6, 9813−9827

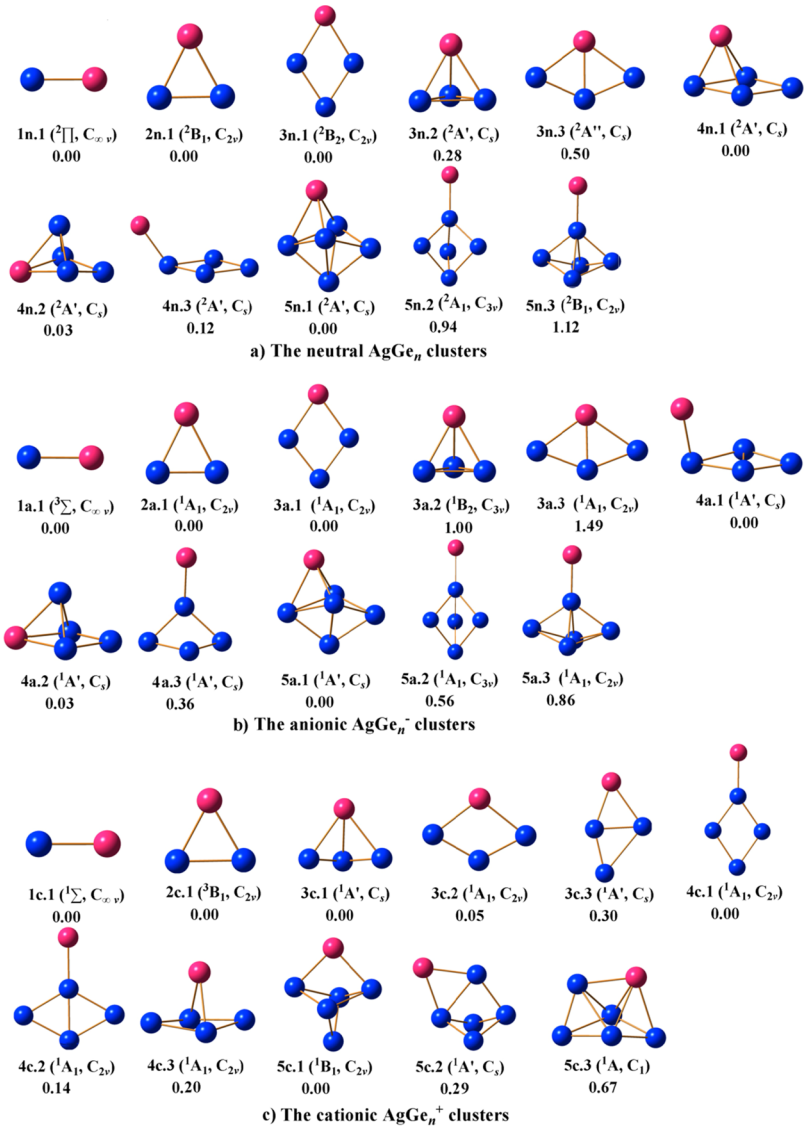

Figure 1. Shapes, electron states, and relative energies (ΔE, eV) of the lower-lying isomers $AgGe_n$ with n = 1−5 at (a) neutral, (b) anionic, and (c) cationic states.

molecular clusters to solve the realistic chemical problems.[57] Therefore, we believe that the results evaluated using the ABCluster global search technique and the mPW2PLYP functional should be reliable.

3. RESULTS AND DISCUSSION

The structures of the optimized geometries of the neutral $AgGe_n$, cationic $AgGe_n^+$, and anionic $AgGe_n^-$ systems, their relative energies, the electronic states, and symmetries are shown in Figures 1−4. For the neutral $AgGe_n$ (n = 1−13), all the ground states are evaluated to be a doublet; For the cationic state, its lower-lying isomers are calculated to be single except $AgGe_2^+$, which is simulated to be a triplet; for the anionic state, the ground state is also simulated to be single except $AgGe^-$, which is simulated to be a triplet.

3.1. Lower-Lying Isomers of $AgGe_n$ Clusters and Their Growth Mechanism. From Figures 1−4, it can be seen that the lowest structure and some of its isomers for neutral and charged $AgGe_n$ (n = 1−13) are carefully selected. Isomers are denoted as nX.Y in which n is the size of Ge_n, X = n, c, and a stand for a neutral, cation, and anion, respectively, and Y = 1, 2, 3...is arranged in an ascending energy order of the isomers.

***n* = 1:** AgGe, $AgGe^+$, and $AgGe^-$. For AgGe, the ground state **1n.1** is characterized by the $^2\prod$ electron state with $[1\sigma^2 2\sigma^2 1\pi^4 1\delta^2 2\delta^2 3\sigma^2 2\pi^1]$ valence electronic configuration in which a bond distance of 2.453 Å is in good agreement with the experimental value of 2.54 Å.[65] After attaching an electron, the high spin state $^3\sum$: $[1\sigma^2 2\sigma^2 1\pi^4 1\delta^2 2\delta^2 3\sigma^2 2\pi^2]$ is calculated to be the ground state of $AgGe^-$ (**1a.1**). Following the detachment of one electron, the close shell electronic state $^1\sum$: $[1\sigma^2 2\sigma^2 1\pi^4 1\delta^2 2\delta^2 3\sigma^2]$ becomes the ground state of $AgGe^+$ (**1c.1**). The bond lengths of **1a.1** and **1c.1** are calculated to be 2.465 and 2.452 Å, showing that gaining or losing an electron has little effect on the bond length of AgGe.

***n* = 2:** $AgGe_2$, $AgGe_2^+$, and $AgGe_2^-$. A triangular structure **2n.1** with C_{2v} symmetry is found for $AgGe_2$ in which the Ag atom connects with two Ge atoms. For the charged species, the structures of $AgGe_2^-$ and $AgGe_2^+$ are almost unchanged. The anion $AgGe_2^-$ exhibits the C_{2v} ($^1A_1$) structure **2a.1** with a closed shell electronic configuration, and cation $AgGe_2^+$ is found to be the $^3B_1$ electron state **2c.1** with C_{2v} symmetry.

https://doi.org/10.1021/acsomega.1c00501
ACS Omega 2021, 6, 9813−9827

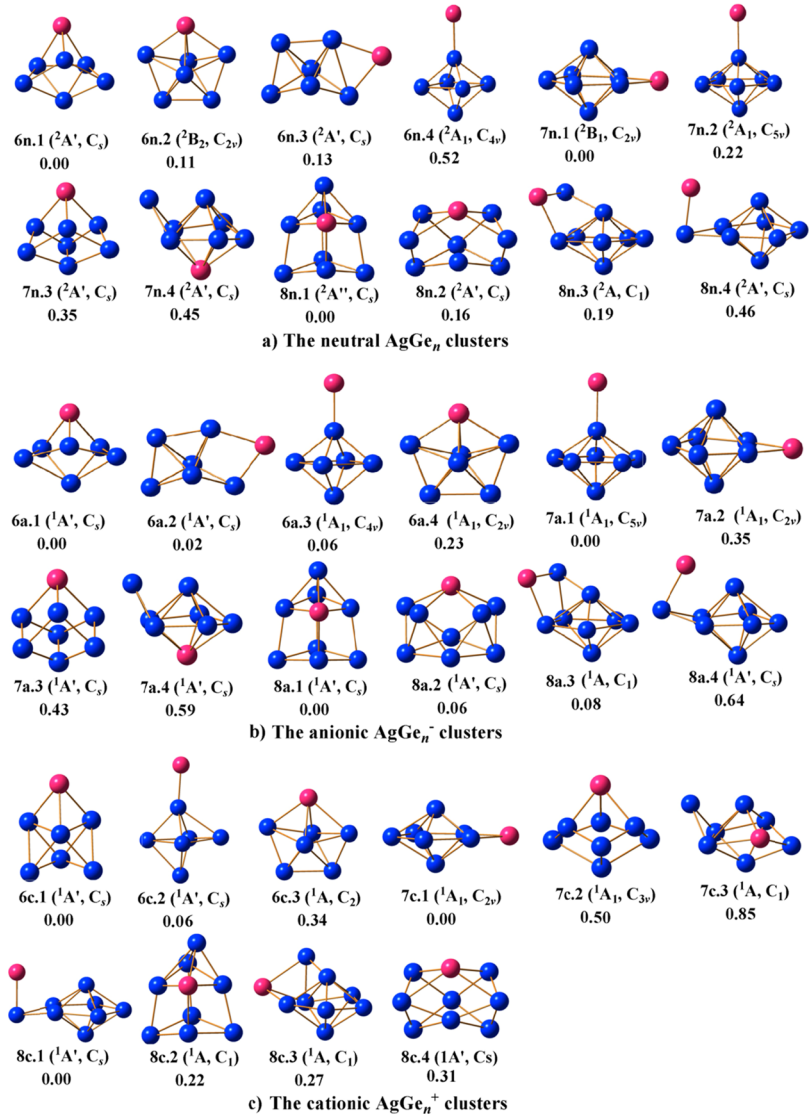

Figure 2. Shapes, electron states, and relative energies (ΔE, eV) of the lower-lying isomers $AgGe_n$ with $n = 6-8$ at (a) neutral, (b) anionic, and (c) cationic states.

***n* = 3:** $AgGe_3$, $AgGe_3^+$, and $AgGe_3^-$. For $AgGe_3$, the C_{2v} symmetry planar rhombus of the $^2A_1$ electronic state is predicted to be the ground state (**3n.1**). The isomer **3n.2** in the C_s point group with an $^2A'$ electronic state can be viewed as attaching an Ag atom to the face of the most stable Ge_3 structure,[2] which is less stable by 0.28 eV in energy than **3n.1**. Following attachment of one electron to form the anionic species, the ground state (**3a.1**) shape of $AgGe_3^-$ remains unchanged. In the cationic state, the lowest-energy structure of $AgGe_3^+$ is a three-dimensional structure **3c.1** (C_s,$^1A'$), which corresponds to the neutral structure **3n.2**. Isomer **3c.2** (C_{2v},$^1A_1$) has a planar shape, which can be viewed as one Ge atom capped in the edge of **2c.1**. Interestingly, the **3c.2** in energy is only less stable than the **3c.1** by 0.05 eV, which means that they compete for the ground state of $AgGe_3^+$.

***n* = 4:** $AgGe_4$, $AgGe_4^+$, and $AgGe_4^-$. For $AgGe_4$, isomer **4n.1** and **4n.2** both have the C_s symmetry and $^2A'$ electronic state. Isomer **4n.1** can be considered as attaching an Ag atom to the face of the most stable Ge_4 structure,[2] and isomer **4n.2** can be considered as attaching a Ge atom to the face of the most stable $AgGe_3$ structure. Isomer **4n.1** is the lowest-energy isomer, being only 0.03 eV lower than **4n.2**, which means both of them compete for the ground state. In the anionic state, the energy of isomer **4a.1** and **4a.2** is also degenerate with an energy gap of 0.03 eV, meaning that the potential energy surface of $AgGe_4$ is relatively shallow. The analysis of simulated PES (see below) indicates that both can coexist in laboratory. The structures of isomer **4a.1** and **4a.2** are both C_s symmetry and $^1A'$ electronic state. For the cationic state, the C_{2v} symmetry plane geometry of the $^1A_1$ electronic state is predicted to be the ground state (**4c.1**) in which an Ag atom attached on the top of the most stable rhombus Ge_4 structure.[2]

***n* = 5:** $AgGe_5$, $AgGe_5^+$, and $AgGe_5^-$. The $AgGe_5$ neutral exhibits a C_s symmetry ground state **5n.1**, which can be regarded as an Ag atom capping one face of the most stable Ge_5.[2] After getting one extra electron, the geometry of the corresponding anion has no significant changes. The ground state **5a.1** with C_s symmetry is more stable in energy than that of isomer **5a.2** and **5a.3** by 0.56 and 0.86 eV, respectively. For the cationic state, the most stable geometry **5c.1** of $AgGe_5^+$ has

https://doi.org/10.1021/acsomega.1c00501
ACS Omega 2021, 6, 9813−9827

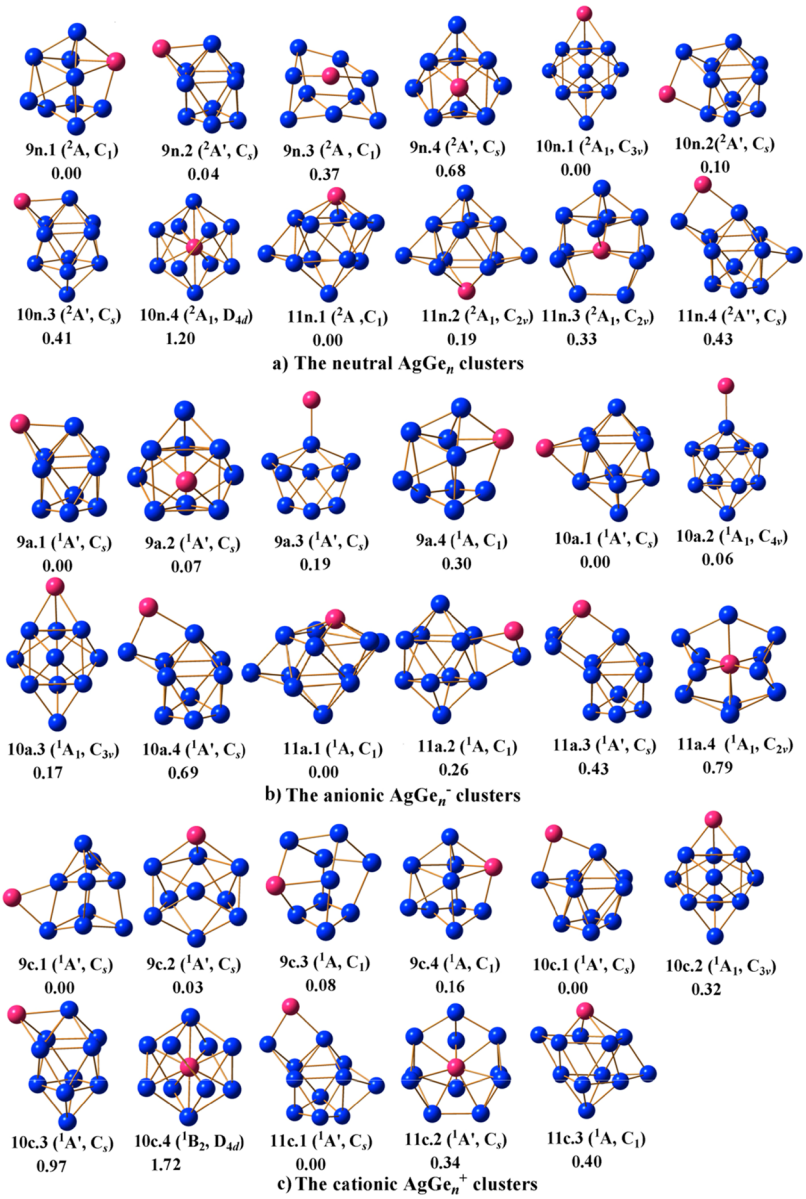

Figure 3. Shapes, electron states, and relative energies (ΔE, eV) of the lower-lying isomers $AgGe_n$ with n = 9−11 at (a) neutral, (b) anionic, and (c) cationic states.

the C_{2v} symmetry with the $^1B_1$ electronic state, which corresponds to the **5n.1**.

***n* = 6:** $AgGe_6$, $AgGe_6^+$, and $AgGe_6^-$. $AgGe_6$ has a C_s ($^2A'$) lowest-energy structure **6n.1**, which can be regarded as attaching an Ag atom to the face of the ground state *tetragonal bipyramid* Ge_6.[2] The lowest stable geometries of the anion $AgGe_6^-$ (**6a.1**) and cation $AgGe_6^+$ (**6c.1**) are almost unchanged as compared to the neutral structure of **6n.1**. Interestingly, the degenerate equilibrium ground states are both found in the anionic and cationic state. Energetically, isomer **6a.2** is only less stable than **6a.1** by 0.02 eV for anion $AgGe_6^-$, and isomer **6c.2** also is only less stable than **6c.1** by 0.06 eV for cation $AgGe_6^+$. Isomer **6a.2** and **6c.2** both can be regarded as attaching an Ag atom to the edge and the top of the most stable Ge_6 structure.[2] The analysis of simulated PES (see below) indicates that the **6a.1** configuration is the ground-state structure.

***n* = 7:** $AgGe_7$, $AgGe_7^+$, and $AgGe_7^-$. For $AgGe_7$, the structure of the ground state **7n.1** (C_{2v}, $^2B_1$) and isomer **7n.2** (C_{5v},$^2A_1$) is 0.22 eV higher in energy as compared to **7n.1**, and both can be considered as an Ag atom capping on the edge and the apex of Ge_7 *pentagonal bipyramid*,[2] respectively. The isomer **7n.4**, which is considered the most stable structure in ref 19., is 0.45 eV higher in energy than **7n.1**. Following attachment of one electron, the C_{5v} symmetry structure **7a.1**, which corresponds to the neutral **7n.2**, acts as the ground state for $AgGe_7^-$. For the cationic state, the geometry of the best isomer for $AgGe_7^+$ is the same as that of the neutral **7n.1**. The C_{2v} symmetry state **7c.1** ($^1A_1$) is more stable in energy than that of isomer **7c.2** and **7c.3** by 0.50 and 0.85 eV, respectively.

***n* = 8:** $AgGe_8$, $AgGe_8^+$, and $AgGe_8^-$. The best isomer of neutral $AgGe_8$ (**8n.1**) with C_s symmetry and $^2A''$ electronic state can be seen as attaching an Ag atom to the face of the *capped pentagonal bipyramid* Ge_8.[2] The next isomer **8n.2** (C_s,$^2A'$), being 0.16 eV less stable than **8n.1**, can be viewed as a distorted Ge_8 *quadrangular prism* with a capped Ag atom on one face. Two other isomers **8n.3** (C_1,^2A) and **8n.4** (C_s,$^2A'$), which are both formed by adding one Ge atom into the

https://doi.org/10.1021/acsomega.1c00501
ACS Omega 2021, 6, 9813−9827

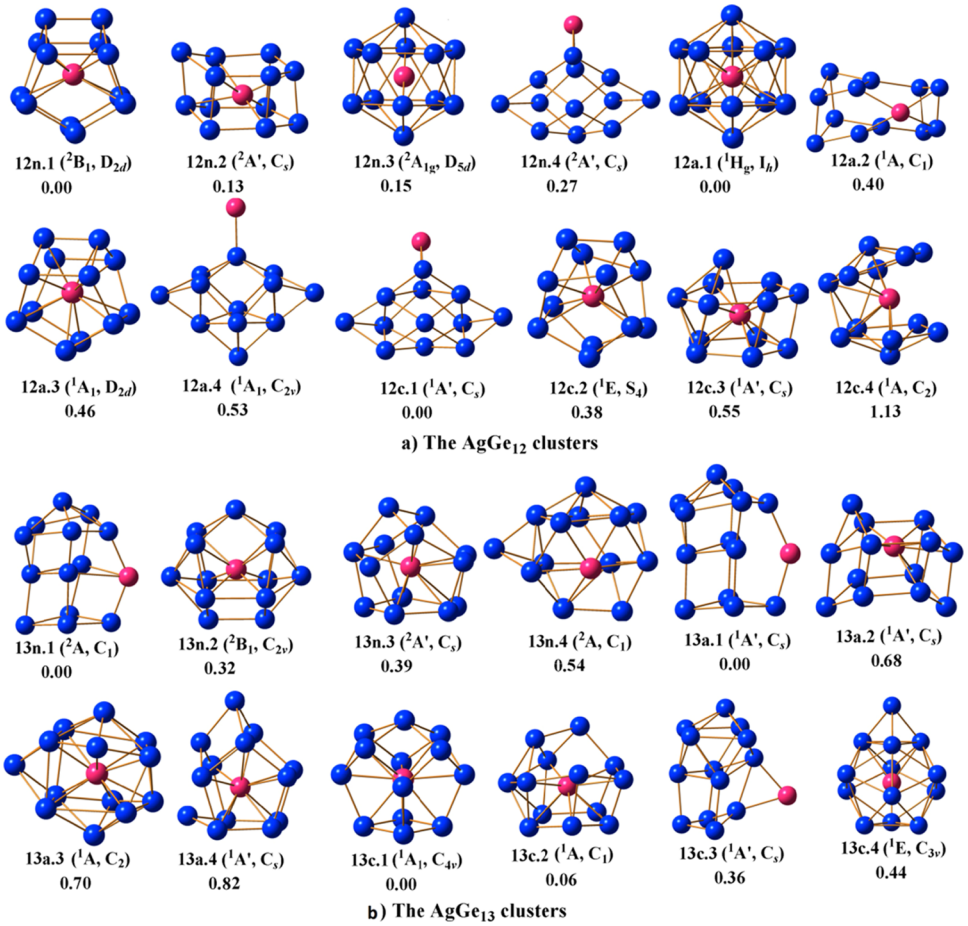

Figure 4. Shapes, electron states, and relative energies (ΔE, eV) of the lower-lying isomers of (a) $AgGe_{12}$ and (b) $AgGe_{13}$.

pentagonal bipyramid Ge_7 and then attaching one Ag atom, are 0.19 and 0.46 eV less stable, respectively, in energy than **8n.1**. For anion $AgGe_8^-$, the isomer **8a.1** (C_s,^{1}A′), corresponding to neutral **8n.1**, is only 0.06 eV lower in energy than **8a.2** (corresponds to the neutral **8n.2**). Although isomer **8a.1** has the lowest energy, we consider that **8a.2** is the best candidate for the ground-state structure through the comparison of the calculated and experimental PES (see below). In the cationic state, the C_s symmetry and ^{1}A″ electronic state **8c.1**, which corresponds to neutral **8n.3**, is calculated as the lowest-energy structure of $AgGe_8^+$. The next isomer **8c.2** (C_1,^{1}A), which is a distorted form of **8n.1**, is less stable in energy than the **8c.1** by 0.22 eV.

***n* = 9:** $AgGe_9$, $AgGe_9^+$, and $AgGe_9^-$. For the neutral $AgGe_9$, two degenerate structures, **9n.1** (C_1,^{2}A) and **9n.2** (C_s,^{2}A′), are found within an energy gap of 0.04 eV. Isomer **9n.1** is formed by adding one Ge atom on the face of the most stable structure $AgGe_8$. Isomer **9n.2** also can be viewed as attaching an Ag atom to the *tricapped trigonal prism* Ge_9.[2] The isomer **9n.3**, which is reported as the most stable structure in ref 19., is 0.37 eV higher in energy than **9n.1**. For the anion, the geometries of the ground state **9a.1** for $AgGe_9^-$ have the same structures corresponding to neutral **9n.2**. The best isomer **9a.1** (C_s,^{1}A′) is 0.30 eV lower in energy than the isomer **9a.4** (corresponding to neutral **9n.1**). In the cationic state, the most stable structure **9c.1** (C_s,^{1}A′), which is formed by adding an Ag atom on the edge of the most stable structure Ge9,[2] is 0.16 eV more stable in energy than the isomer **9c.4** (corresponding to neutral **9n.1**).

***n* = 10:** $AgGe_{10}$, $AgGe_{10}^+$, and $AgGe_{10}^-$. The C_{3v} symmetry structure of the ^{2}A$_1$ electronic state is predicted to be the ground state (**10n.1**) for $AgGe_{10}$. It is formed by either adding one Ge atom into the face of structure **9n.2** or adsorbing an Ag atom on the face of the *tetracapped trigonal prism* Ge_{10}.[2] The isomer **10n.3**, which is predicted to be the most stable structure in ref 19., is 0.41 eV higher in energy than **10n.1**. In the anionic state, the most stable structure **10a.1** with C_s symmetry and ^{1}A′ electronic state is formed by adding an Ag atom on the face of *bicapped tetragonal antiprism* Ge_{10}. The isomer **10a.2** with C_{4v} symmetry and ^{1}A$_1$ electronic state can be formed by attaching an Ag atom on the vertex of the *bicapped tetragonal antiprism* Ge_{10}. It is only less stable than **10a.1** by 0.06 eV in energy. Simulated PES analysis shows that both isomers can exist (see below). For cationic clusters, the ground-state isomer **10c.1** with C_s symmetry (^{1}A′) can also be derived by adding an Ag atom on a different face of the *tetracapped trigonal prism* Ge_{10}.

***n* = 11:** $AgGe_{11}$, $AgGe_{11}^+$, and $AgGe_{11}^-$. For $AgGe_{11}$, the C_1 structure **11n.1**, which can be viewed as distorted by a substitution of an Ag atom for a Ge atom of icosahedral-like Ge_{12}, is found to be the global minima of the cluster. The isomer **11n.2** with C_{2v} symmetry (^{2}A$_1$), which is reported as the most stable structure in ref 19., is 0.19 eV higher in energy than **11n.1**. Isomer **11n.3** with C_{2v} symmetry (^{2}A$_1$) is an Ag-encapsulated into Ge_{11} cage, being 0.33 eV higher in energy than **11n.1**. Following the attachment of one electron, the most stable structure **11a.1**, corresponding to neutral **11n.1**, has the C_1 symmetry and ^{1}A electronic state. The cage

https://doi.org/10.1021/acsomega.1c00501
ACS Omega 2021, 6, 9813−9827

structure **11a.4** (C_{2v},$^1A_1$) is less stable in energy than **11a.1** by 0.79 eV. For the cationic state, the ground state **11c.1** of $AgGe_{11}^+$ is formed by attaching the additional Ge atom on the face of **10c.1**. The structure **11c.2**, which is a slightly distorted form of neutral cage structure **11n.3**, is less stable in energy than **11c.1** by 0.34 eV.

***n* = 12:** $AgGe_{12}$, $AgGe_{12}^+$, and $AgGe_{12}^-$. The ground state **12n.1** of neutral $AgGe_{12}$ is an endohedral structure with D_{2d} symmetry in which an Ag atom is located inside a Ge_{12} cage. The isomer **12n.3** is D_{5d} symmetric icosahedron-like in which an Ag atom is located inside a dicapped pentagonal antiprism cage. The isomer **12n.3** is 0.15 eV higher in energy relative to **12n.1**. Following attachment of one electron, the ground state **12a.1** of $AgGe_{12}^-$, which corresponds to neutral **12n.3**, has a high I_h (^1H_g) symmetric icosahedral structure. This structure is similar to that of the $AuGe_{12}^-$ reported by Zheng in the series of studies on Au-doped Ge_n clusters.[26] For the cationic state, the geometry of the best isomer **12c.1** for $AgGe_{12}^+$ is an exohedral structure with C_s symmetry and $^1A'$ electronic state, which can be viewed as attaching an Ag atom to the face of *hexcapped trigonal prism* Ge_{12}.[2] Isomers **12c.2**, **12c.3**, and **12c.4** are all cage structures, being 0.38, 0.55, and 1.13 eV higher in energy than **12c.1**, respectively.

***n* = 13:** $AgGe_{13}$, $AgGe_{13}^+$, and $AgGe_{13}^-$. The most stable structure **13n.1** of neutral $AgGe_{13}$ is not a cage configuration but an exohedral structure, which can be viewed as replacing a Ge atom of the most stable structure of Ge_{14}[3] with an Ag atom. The best isomer **13n.1** with C_1 symmetry is more stable in energy than the cage structure **13n.2** and **13n.3** by 0.32 and 0.39 eV, respectively. Isomer **13n.4** also is a no-cage structure with C_1 symmetry, which is reported as the lowest-energy configuration in the literature,[19] but here it is 0.54 eV higher than **13n.1**. For $AgGe_{13}^-$, the ground state **13a.1** (corresponding to the neutral ground state **13n.1**) with C_s symmetry and $^1A'$ electronic state also is an exohedral structure. The isomer **13a.1** is more stable than the endohedral isomer **13a.2**, **13a.3**, and **13a.4** by 0.68, 0.70, and 0.82 eV, respectively. For $AgGe_{13}^+$, the ground state **13c.1** with C_{4v} symmetry is calculated to be an endohedral structure, which is a capped fullerene-like cage. The next isomer **13c.2**, which can be considered as the Ag-encapsulated into Ge_{13} cage of the *dimer-capped pentagonal-hexagonal prism*, is less stable than **13c.1** by 0.06 eV energetically.

3.2. Growth Pattern. Based on the structural features of the determined global minimum structure, the growth mechanism for the clusters $AgGe_n$ with n = 1−13 emerges as follows: For neutral clusters, the most stable forms of $AgGe_n$ except the $AgGe_{12}$ definitely prefer an exohedral structure, which is formed by attaching an Ag atom to a Ge_n cluster or a Ge atom to an $AgGe_{n-1}$ cluster when n = 1−10, and when n = 13, it is formed by replacing a Ge atom of a Ge_{n+1} cluster with an Ag atom. For anionic states, although the lowest-energy structures of $AgGe_n^-$ at n = 7−10 are different from the corresponding neutral clusters, the growth patterns of most stable structures are consistent. For cationic states, the global minimal structures of $AgGe_n^+$ with n ranging from 1 to 12 are formed by attaching an Ag atom to the Ge_n cluster or a Ge atom to the $AgGe_{n-1}$ cluster, and the endohedral structure becomes the ground-state configuration when n = 13. The ground-state configurations of $AgGe_n^+$ are different from the corresponding neutral ground-state structure when n = 3, 4, and 8−13.

3.3. Photoelectron Spectra. By comparing the PES obtained by theoretical calculation and experiment, it can not only verify the accuracy of the ground-state structure predicted by the theoretical calculation, but also explain the reliability of the theoretical calculation scheme. In this section, the PES of the ground-state isomers for $AgGe_n^-$ (n = 2−13) are simulated based on the generalized Koopmans' theorem (denoted as ΔDFT) combined with Multiwfn software[68] and compared with experimental data.[22] First, the VDE which corresponds to the first peak of PES and the adiabatic electron affinity (AEA) of experiment and simulation are compared and listed in Table 2. Then, the number of other peaks and their relative locations

Table 2. Theoretical and Experimental VDEs and AEAs for $AgGe_n^-$ (n = 1−13)

	VDE		AEA	
n	theor	exptl[a]	Theor	exptl[a]
1	1.50(1.47)		1.50(1.47)	
2	2.13(2.08)	2.11 ± 0.08	2.08(2.05)	1.97 ± 0.08
3	2.71(2.65)	2.74 ± 0.08	2.55(2.51)	2.50 ± 0.08
4	2.62(2.58)	2.65 ± 0.08	2.34(2.30)	2.39 ± 0.08
5	2.98(2.93)	3.02 ± 0.08	2.62(2.58)	2.73 ± 0.08
6	2.70(2.63)	2.70 ± 0.08	2.37(2.35)	2.43 ± 0.08
7	2.93(2.87)	2.99 ± 0.08	2.45(2.37)	2.71 ± 0.08
8	3.24(3.16)	3.27 ± 0.08	2.75(2.67)	2.97 ± 0.08
9	3.47(3.40)	3.59 ± 0.08	3.07(3.02)	3.06 ± 0.08
10	3.54(3.40)	3.64 ± 0.20	2.98(2.94)	3.22 ± 0.20
11	3.32(3.27)	3.37 ± 0.20	3.05(2.99)	3.06 ± 0.20
12	3.48(3.41)	3.68 ± 0.20	3.19(3.31)	3.34 ± 0.20
13	3.86(3.74)	4.04 ± 0.20	3.56(3.48)	3.45 ± 0.20

[a]From ref 22.; The values in parentheses are calculated at the mPW2PLYP/aug-cc-pVTZ-pp.

are matched by the simulated PES and experimental one. The simulated PES of the most stable structures and experimental spectra are displayed in Figure 5.

As shown in Figure 5, the simulated PES of the **2a.1** have two different peaks (X and A) within ≤4.5 eV located at 2.13 and 3.39 eV, which are in concordance with the experimental data of 2.11 and 3.70 eV.[22] From the PES of $AgGe_3^-$, it can be seen that simulated PES of the **3a.1** have three adjacent peaks (X, A, and B) located at 2.71, 2.94, and 3.19 eV. The first and third peak's positions can be consistent with the experimental values of 2.74 and 3.13 eV. For $AgGe_4^-$, the simulated PES of the **4a.1** and **4a.2** have three distinct peaks (X, A, and B) situated at 2.62, 3.62, and 3.98 eV and 2.59, 3.27, and 3.76 eV, respectively. They are in concordance with the experimental data of 2.65, 3.27, and 3.68 eV, respectively. Therefore, we suggest that two energy degenerate isomers **4a.1** and **4a.2** coexist in the experiment. For the simulated PES of **5a.1**, there are four peaks (X, A, B, and C) located at 2.98, 3.31, 3.74, and 4.16 eV, which is in good accordance with the experimental data of 3.02, 3.50, 3.85, and 4.22 eV,[22] respectively. For $AgGe_6^-$, two PES are simulated. The simulated PES of the **6a.1** have three distinct peaks (X, A, and B) situated at 2.71, 3.59, and 4.08 eV, which are in excellent agreement with the experimental values of 2.70, 3.58, and 3.94 eV,[22] respectively. The simulated PES of the **6a.2** have two distinct peaks (X and B) situated at 2.58 and 3.93 eV. Although they are in concordance with the experimental data of 2.70 and 3.94 eV, the number of peaks is obviously insufficient. The simulated PES of the **7a.1** have two different peaks (X and A) within

https://doi.org/10.1021/acsomega.1c00501
ACS Omega 2021, 6, 9813−9827

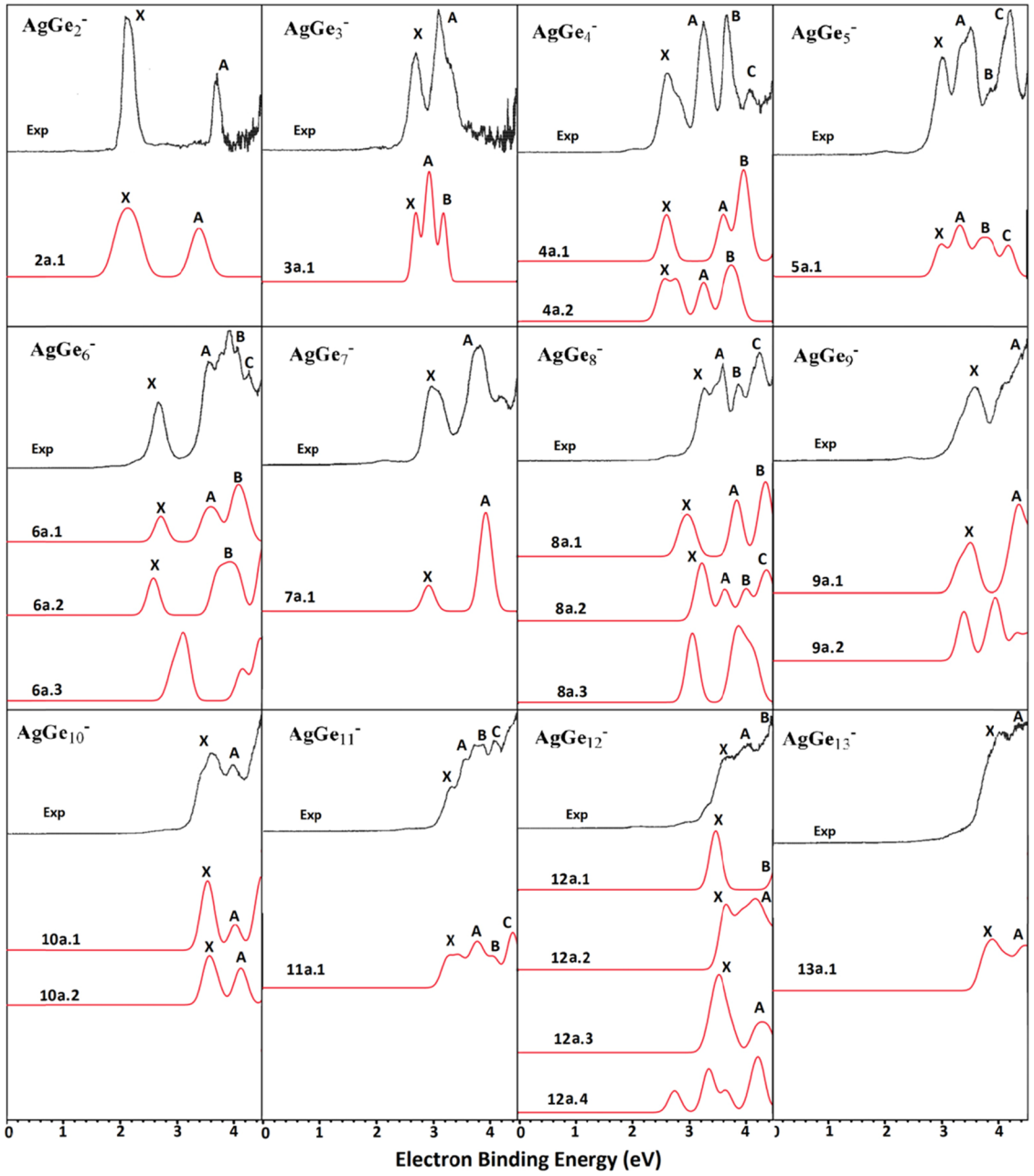

Figure 5. Simulated PES spectra of the lowest-lying energy structures of $AgGe_n^-$ (n = 2−13) clusters. Experimental PES reprinted with permission from ref 22.

≤4.5 eV located at 2.93 and 3.93 eV, which are in concordance with the experimental data of 2.99 and 3.80 eV.[22] For $AgGe_8^-$, there are four different peaks (X, A, B, and C) located at 3.24, 3.64, 4.02, and 4.38 eV in the simulated PES of **8a.2**, which well reproduce the experimental values[22] of 3.27, 3.62, 3.88, and 4.25 eV, respectively. The spectrum of isomer **8a.1** has three distinct peaks (X, A, and B) situated at 2.98, 3.86, and 4.36 eV, which can be ruled out of the most stable structure of $AgGe_8^-$. For $AgGe_9^-$, two distinct peaks located at 3.47 and 4.33 eV are obtained in the simulated PES of **9a.1**, and they are in reasonable agreement with the experimental values of 3.59 and 4.38 eV.[22] For $AgGe_{10}^-$, two distinct peaks located at 3.54 and 4.02 eV and 3.57 and 4.11 eV are obtained in the simulated PES of **10a.1** and **10a.2**, respectively. They agree with the experimental values of 3.64 and 4.03 eV, respectively.[22] It is to say that these two energy degenerate isomers may coexist in the experiment. Four peaks for simulated PES of **11a.1** are situated at 3.32, 3.79, 4.04, and 4.41 eV, which are in excellent agreement with the experimental data of 3.37, 3.61, 3.90, and 4.15 eV,[22] respectively. Although Kong[22] pointed out that the peak shape of experimental PES of $AgGe_{12}^-$ was wide and it was difficult to observe a clear peak because of the overlap of energy levels, three peaks (X, A, and B) can be roughly assigned to 3.68, 4.11, and 4.50 eV. It is interesting that the simulated PES of **12a.1** have two resolved peaks (X and B) centered at 3.48 and 4.61 eV, which is in good accordance with the experimental data of 3.68 (X) and 4.50 (B) eV,[22] while the simulated PES of **12a.2** and **12a.3** also have two distinct peaks (X and A) situated at 3.67 and 4.18 eV and 3.54 and 4.30 eV, respectively. They are in concordance with the experimental data of 3.68 (X) and 4.11 (A) eV, respectively. In this case, one

https://doi.org/10.1021/acsomega.1c00501
ACS Omega 2021, 6, 9813−9827

cannot determine which isomer is the ground-state structure. Therefore, we highly suggest that the experimental PES of $AgGe_{12}^-$ should be further examined. The simulated PES of **13a.1** have two major features centered at 3.86 and 4.45 eV, which are in reasonable agreement with the experimental values of 4.04 and 4.38 eV.[22]

3.4. EAs and IP. From Table 2, it can be concluded that the first theoretical VDEs of $AgGe_n^-$ (n = 2−13) show a good agreement with available experimental values.[22] The average absolute deviation of them is 0.07 (0.14) eV (the value in parentheses is calculated at the mPW2PLYP/aug-cc-pVTZ-PP//mPW2PLYP/cc-pVTZ-PP level). The largest deviation is 0.20 eV for $AgGe_{12}$, which is within experimental errors of 0.20 eV. For the AEAs, the quantitative analysis suggests that the mean absolute deviation of simulated of $AgGe_n$ (n = 2−13) from the experimental data is 0.11 (0.12) eV. The largest error is $AgGe_7$ and $AgGe_{10}$, which is off by 0.26 and 0.24 eV, respectively. The reason may be that their experimental PES exhibit a featureless long and very rounded tail, which means that it is difficult to determine the exact AEA value. If $AgGe_7$ and $AgGe_{10}$ are removed, the average absolute deviations are only 0.09 eV. All these show that our theoretical method is reliable and once again confirms that the ground-state configurations in this paper are accurate.

Vertical ionization potential (VIP) and adiabatic ionization potential (AIP), as important chemical and physical quantities, are discussed in this section. The VIP [defined as the difference of total energies as follows: VIP = E(cation at optimized neutral geometry) − E(optimized neutral)] and AIP [defined as the difference of total energies in following manner: VIP = E(optimized cation) − E(optimized neutral)] of neutral $AgGe_n$ cluster and pure Ge_{n+1} clusters are calculated and listed in Table 3. No experimental IP of $AgGe_n$ is available for comparison. Therefore, we compared the IP of $AgGe_n$ with that of pure Ge_n clusters as shown in Figure 6. From Figure 6, it can be found that (i) The IP with two different types of VIP and AIP for $AgGe_n$ clusters is lower than that of pure Ge_{n+1} clusters, respectively, meaning that doping an Ag atom in neutral Ge_n clusters will decrease their IP. (ii) For $AgGe_n$ (n = 1−13) clusters, the highest VIP and AIP values are calculated to be 7.71 eV for $AgGe_3$ and 7.07 eV for $AgGe_2$, respectively. $AgGe_7$ and $AgGe_{10}$ present the minimum values of VIP and AIP by 5.91 and 5.68 eV, respectively. (iii) For Ge_{n+1} (n = 1−13) clusters, the calculated values of VIP are in good agreement with the experimental data,[5] and their average absolute deviation is only 0.08 (0.09) eV.

3.5. Binding Energy and Relative Stability. The relative stabilities of the most stable structures of $AgGe_n^{\lambda}$ (λ = −1, 0, and +1; n = 1−13) clusters are examined in terms of both binding energy per atom (E_b) and second-order difference in energy (Δ^2E). $E_b(AgGe_n^{\lambda})$ and $\Delta^2E(AgGe_n^{\lambda})$ are defined as the following reactions:

$$E_b(AgGe_n) = [nE(Ge) + E(Ag) - E(AgGe_n)]/(n+1) \quad (1)$$

$$E_b(AgGe_n^+) = [(n-1)E(Ge) + E(Ge^+) + E(Ag) - E(AgGe_n^+)]/(n+1) \quad (2)$$

$$E_b(AgGe_n^-) = [(n-1)E(Ge) + E(Ge^-) + E(Ag) - E(AgGe_n^-)]/(n+1) \quad (3)$$

Table 3. VIP and AIP of $AgGe_n$ and Ge_{n+1} (n = 1−13) Clusters

cluster	VIP (eV)	AIP (eV)	Cluster	VIP (eV)	expt. of VIP	AIP (eV)
AgGe	7.05 (7.02)	7.05 (7.02)	Ge_2	7.57 (7.52)	7.58−7.76 (7.67)[a]	7.57 (7.51)
$AgGe_2$	7.07 (7.03)	7.07 (7.03)	Ge_3	8.01 (7.96)	7.97−8.09 (8.03)[a]	7.92 (7.87)
$AgGe_3$	7.71 (7.67)	6.89 (6.84)	Ge_4	7.80 (7.76)	7.87−7.97 (7.92)[a]	7.53 (7.48)
$AgGe_4$	6.70 (6.64)	6.33 (6.32)	Ge_5	7.96 (7.91)	7.87−7.97 (7.92)[a]	7.79 (7.75)
$AgGe_5$	7.17 (7.11)	6.61 (6.54)	Ge_6	7.76 (7.72)	7.58−7.76 (7.67)[a]	7.36 (7.33)
$AgGe_6$	6.63 (6.57)	6.25 (6.23)	Ge_7	7.89 (7.84)	7.58−7.76 (7.67)[a]	7.55 (7.51)
$AgGe_7$	5.91 (5.88)	5.70 (5.67)	Ge_8	7.01 (6.94)	6.72−6.94 (6.83)[a]	6.61 (6.53)
$AgGe_8$	6.64 (6.54)	6.17 (6.09)	Ge_9	7.20 (7.09)	7.06−7.24 (7.15)[a]	7..1 (6.94)
$AgGe_9$	6.42 (6.34)	6.05 (5.94)	Ge_{10}	7.55 (7.45)	7.46−7.76 (7.61)[a]	7.38 (7.31)
$AgGe_{10}$	6.24 (6.17)	5.68 (5.60)	Ge_{11}	6.59 (6.53)	6.55−6.72 (6.64)[a]	6.34 (6.28)
$AgGe_{11}$	6.46 (6.39)	5.86 (5.81)	Ge_{12}	7.10 (7.00)	6.94−7.06 (7.00)[a]	6.88 (6.83)
$AgGe_{12}$	6.13 (6.82)	5.67 (5.81)	Ge_{13}	7.03 (6.97)	6.94−7.06 (7.00)[a]	6.82 (6.71)
$AgGe_{13}$	6.74 (6.65)	6.06 (5.92)	Ge_{14}	7.14 (7.08)	7.06−7.24 (7.15)[a]	6.86 (6.82)

[a]The data taken from ref 5. and in parentheses are average values; the values in parentheses are calculated at the mPW2PLYP/aug-cc-pVTZ-pp level.

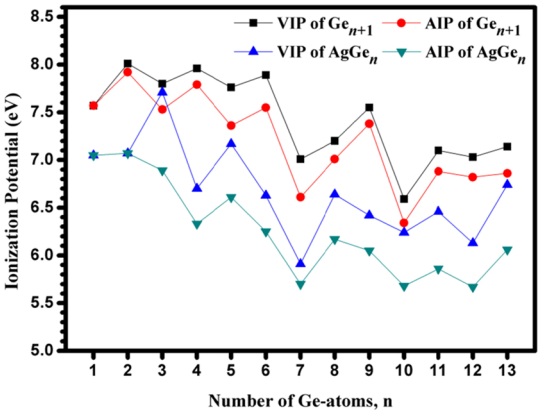

Figure 6. IP of the ground-state structure of $AgGe_n$ and Ge_{n+1} (n = 1−13) clusters.

$$\Delta^2E(AgGe_n^{\lambda}) = E(AgGe_{n-1}^{\lambda}) + E(AgGe_{n+1}^{\lambda}) - 2E(AgGe_n^{\lambda}) \quad (4)$$

Where E(Ag), E(Ge), $E(Ge^+)$, and $E(Ge^-)$ are the total energies of the Ag atom, Ge atom and the charged Ge^+ and Ge^-, respectively. $E(AgGe_n)$, $E(AgGe_n^+)$, and $E(AgGe_n^-)$ are the total energies of the cluster $AgGe_n$ at neutral, cationic, and anionic states, respectively. To understand how the Ag dopant influences the stability of pure Ge_n clusters, the E_b and Δ^2E of Ge_{n+1}^{λ} (λ = −1, 0, and +1; n = 1−13) are further examined and are defined as follows:

$$E_b(Ge_{n+1}^{\lambda}) = [nE(Ge) + E(Ge^{\lambda}) - E(Ge_{n+1}^{\lambda})]/(n+1) \quad (5)$$

https://doi.org/10.1021/acsomega.1c00501
ACS Omega 2021, 6, 9813−9827

$$\Delta^2 E(Ge_{n+1}^{\lambda}) = E(Ge_n^{\lambda}) + E(Ge_{n+2}^{\lambda}) - 2E(Ge_{n+1}^{\lambda}) \quad (6)$$

Where $E(Ge_n^{\lambda})$ are the total energies of neutral, cationic, and anionic Ge_n clusters, respectively. These total energies are calculated through the mPW2PLYP scheme combined with the aug-cc-pVTZ basis set for the most stable structures of neutral and charged Ge_n clusters reported in previous studies.[2,3,9,67] The E_b values are listed in Table 4, and the plots are shown in Figures 7 and 8. The plots of $\Delta^2 E$ are given in Figure 9.

Table 4. Average Binding Energies (E_b, eV) of $AgGe_n^{\lambda}$ and Ge_{n+1}^{λ} (λ = −1, 0, and +1; n = 1−13) Clusters[a]

	E_b					
n	$AgGe_n^-$	$AgGe_n$	$AgGe_n^+$	Ge_{n+1}^-	Ge_{n+1}	Ge_{n+1}^+
1	1.00 (1.00)	0.87 (0.87)	1.26 (1.25)	1.79 (1.77)	1.44 (1.42)	1.57 (1.56)
2	2.00 (1.98)	1.72 (1.70)	1.97 (1.95)	2.44 (2.41)	2.14 (2.12)	2.11 (2.09)
3	2.42 (2.40)	2.09 (2.07)	2.33 (2.31)	2.79 (2.76)	2.63 (2.61)	2.71 (2.68)
4	2.57 (2.55)	2.35 (2.33)	2.65 (2.62)	3.02 (2.99)	2.82 (2.80)	2.83 (2.80)
5	2.88 (2.86)	2.66 (2.63)	2.86 (2.84)	3.11 (3.08)	3.00 (2.98)	3.08 (3.05)
6	2.91 (2.88)	2.75 (2.72)	2.97 (2.94)	3.20 (3.17)	3.11 (3.09)	3.15 (3.13)
7	2.99 (2.96)	2.84 (2.81)	3.10 (3.08)	3.14 (3.10)	3.01 (2.99)	3.17 (3.14)
8	3.03 (3.00)	2.86 (2.84)	3.05 (3.02)	3.24 (3.21)	3.11 (3.08)	3.11 (3.17)
9	3.11 (3.09)	2.93 (2.90)	3.11 (3.09)	3.31 (3.28)	3.23 (3.20)	3.27 (3.25)
10	3.18 (3.15)	3.02 (2.99)	3.22 (3.19)	3.25 (3.22)	3.15 (3.12)	3.29 (3.26)
11	3.15 (3.12)	3.00 (2.97)	3.16 (3.13)	3.23 (3.20)	3.16 (3.13)	3.24 (3.21)
12	3.17 (3.16)	3.02 (3.00)	3.18 (3.15)	3.27 (3.24)	3.16 (3.13)	3.24 (3.22)
13	3.22 (3.19)	3.05 (3.02)	3.18 (3.16)	3.28 (3.26)	3.22 (3.19)	3.29 (3.26)

[a]The values in parentheses are calculated at the mPW2PLYP/aug-cc-pVTZ-pp level.

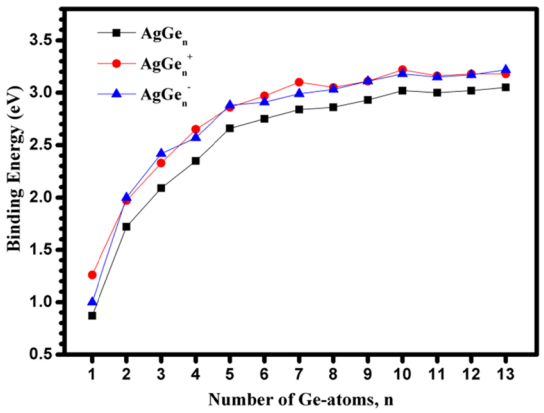

Figure 7. Average binding energy (E_b, eV) of $AgGe_n^{\lambda}$ (λ = 0, +1, and −1; n = 1−13) clusters.

From Figures 7 and 8, it can be seen that: (i) The $E_b(AgGe_n^-)$ and $E_b(AgGe_n^+)$ are larger than the corresponding $E_b(AgGe_n)$. This is because $AgGe_n$ clusters possess an open-shell electronic structure. When an electron is obtained or lost, $AgGe_n^-$ (except for $AgGe^-$, the most stable state is a triplet) or $AgGe_n^+$ (except for $AgGe_2^+$, the most stable state is a triplet) clusters have the closed shell electronic structure, enhancing the stability. It should be noted that the simulated binding energy of AgGe is 0.87 eV, which is perfectly in line with the experimental value of 0.89 eV.[66] (ii) Whether it is neutral or charged $AgGe_n$ and Ge_{n+1}, the binding energy is increased with the increase of the cluster sizes. The binding energies of pure Ge_{n+1} and its charged clusters are slightly larger than those of Ag-doped germanium corresponding clusters, respectively, which indicates that doping of an Ag atom may decrease the stability of neutral and charged Ge_{n+1} clusters. (iii) The maximum values of E_b are calculated to be 3.02 eV ($AgGe_{12}$) and 3.05 eV ($AgGe_{13}$) for neutral $AgGe_n$ clusters and 3.23 eV (Ge_{10}) and 3.22 eV (Ge_{14}) for neutral Ge_{n+1} clusters, which indicates that they show a good thermodynamic stability. At the anionic state, the value of E_b is the maximum at n = 10 (3.18 eV) and n = 13 (3.22 eV) for $AgGe_n^-$ clusters and at n = 10 (3.31 eV) and n = 14 (3.28 eV) for Ge_n^- clusters. At the cationic state, $AgGe_{10}^+$ presents the highest E_b value by 3.22 eV for $AgGe_n^+$ clusters, and Ge_{11}^+ and Ge_{14}^+ present the

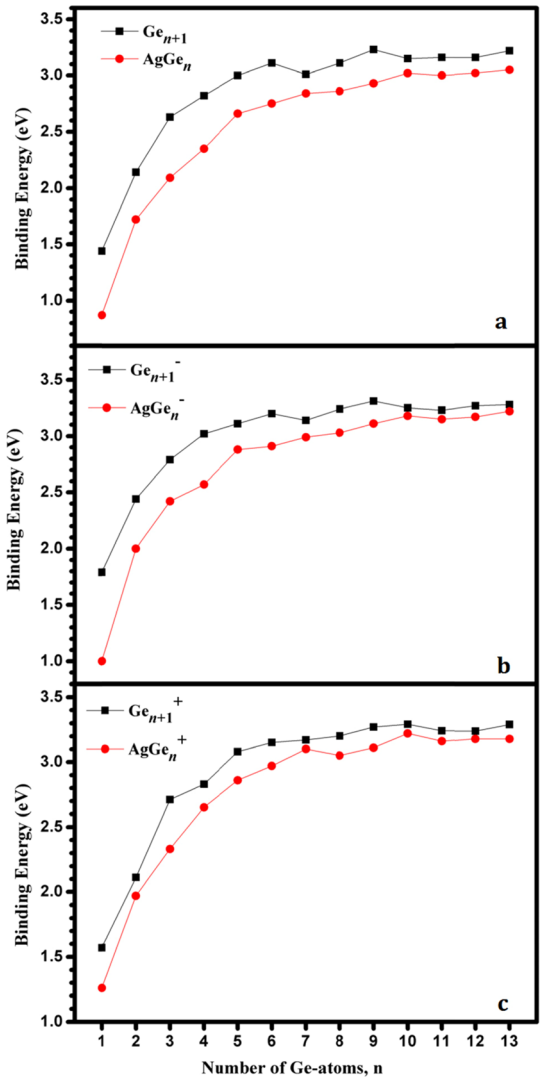

Figure 8. Binding energy (E_b, eV) of $AgGe_n^{\lambda}$ and Ge_{n+1}^{λ} (λ = 0, −1, and +1; n = 1−13) clusters at (a) neutral, (b) anionic, and (c) cationic states.

https://doi.org/10.1021/acsomega.1c00501
ACS Omega 2021, 6, 9813−9827

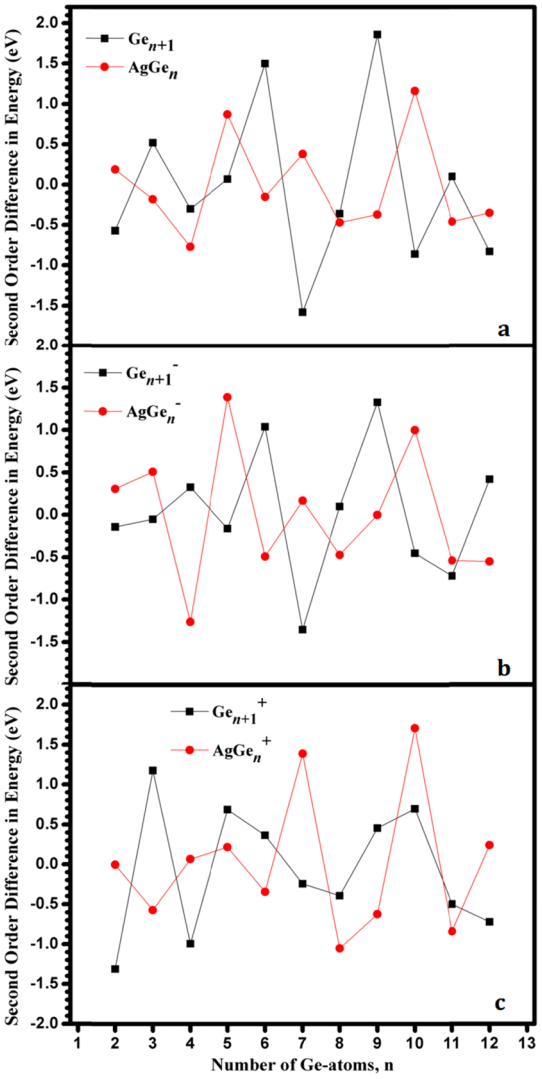

Figure 9. Second-order difference in energy (Δ^2E, eV) of $AgGe_n^{\lambda}$ and Ge_{n+1}^{λ} (λ = 0, −1, and +1; n = 1−13) clusters at (a) neutral, (b) anionic, and (c) cationic states.

highest binding energy at the same value (3.29 eV) for Ge_n^+ clusters.

The second-order difference in energy of the nanoalloy cluster is the feature that reflects the relative stability between one cluster and its two directly adjacent clusters. The higher the value of Δ^2E, the better the relative stability of the cluster. It can be observed from Figure 9 that the Δ^2E for $AgGe_5^{0/-/+}$, $AgGe_7^{0/-/+}$, $AgGe_{10}^{0/-/+}$, $AgGe_{12}^{0/-/+}$, $Ge_4^{0/+}$, $Ge_7^{0/-}$, $Ge_{10}^{0/-}$, Ge_{12}, Ge_5^-, Ge_6^+, and Ge_{11}^+ clusters all have obvious peaks, indicating that their stability is higher than that of the adjacent clusters.

3.6. HOMO-LUMO Gap and Hardness. HOMO-LUMO energy gap (E_{gap}) is an electronic property of clusters, which can be used to express the performance of related chemical properties, such as photochemistry and conductivity. The value of E_{gap} means the minimum energy required to transfer an electron from the HOMO to the LUMO. The value of the HOMO-LUMO gap has an inverse response to the external perturbations, which means that a small value corresponds to a large response. Therefore, the E_{gap} of neutral and charged $AgGe_n^{\lambda}$ (λ = 0, −1, +1; n = 1−13) clusters has been computed using the mPW2PLYP scheme and is pictured in Figure 10. It

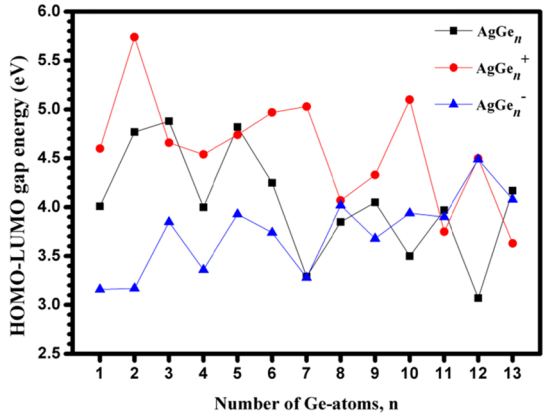

Figure 10. Highest occupied molecular orbital-lowest unoccupied molecular orbital (HOMO-LUMO) energy gap (E_{gap}, eV) of $AgGe_n^{\lambda}$ (λ = 0, −1,+1; n = 1−13) clusters.

can be found that: (i) For neutral clusters, the values of E_{gap} range from 3.07 to 4.88 eV. The maximum value is calculated at $AgGe_3$, and the minimum value is calculated at $AgGe_7$. In anionic states, E_{gap} ranges from 3.16 to 4.49 eV. The maximum value is calculated at $AgGe_{12}^-$, and the minimum value is calculated at $AgGe^-$ and $AgGe_2^-$. For cationic states, it ranges from 3.63 to 5.74 eV. The minimum value is simulated at $AgGe_{13}^+$, and the maximum value is calculated at $AgGe_2^+$. (ii) The E_{gap} of $AgGe_n$ clusters are larger than that of $AgGe_n^-$ clusters with the exception of n = 8 and 12, indicating that an additional electron reduces their chemical stability. Furthermore, after losing an electron, the E_{gap} of $AgGe_n^+$ is narrower than that of $AgGe_n$ for n = 3, 5, and 11−13 and is wider for n = 1, 2, 4, and 6−10.

Hardness (η), as another important parameter reflecting the chemical properties, is calculated for $AgGe_n$ (n = 1−3), and it can be defined as follows:

$$\eta = \frac{\mathrm{IP} - \mathrm{EA}}{2} \tag{7}$$

To facilitate comparison, hardness and HOMO-LUMO gap of $AgGe_n$ are shown in Figure 11 as a function of cluster sizes. To better understand the relationship of changes between them, the comparison of HOMO with VIP and LUMO with VDE is also given in Figure 11. It can be seen from Figure 11 that the trend of E_{gap} and hardness is slightly different. For example, the hardness analysis of AgGe shows that it has a weak chemical reactivity, but HOMO-LUMO gap analysis indicates that it possesses a strong chemical activity. The reason is that the trend of HOMO and VIP is the same. However, the trend of LUMO and VDE is slightly different.

3.7. Charge Transfer and Partial Density of States (PDOS). In this section, NPAs of the most stable structure for $AgGe_n^{\lambda}$ (n = 1−13; λ = −1, 0, and +1) clusters were performed using the mPW2PLYP scheme. The results are shown in Table 5. From Table 5, it can be seen that the valence configurations of the Ag atom in $AgGe_n^{\lambda}$ (n = 1−13; λ = −1, 0, and +1) clusters are $5s^{0.36-1.22}4d^{9.77-9.89}5p^{0.01-2.70}$. Regardless of being neutral or charged, the 4d electrons of Ag atoms are almost unchanged, meaning that the 4d electrons of Ag hardly participate in bonding. The calculated charges of Ag atoms in $AgGe_n$ (n = 1−13) with the exception of n = 1 and 12 are 0.02−0.48 a.u, indicating that Ag atoms mainly act as electron donors. The charges of Ag atoms in anionic clusters are the

https://doi.org/10.1021/acsomega.1c00501
ACS Omega 2021, 6, 9813−9827

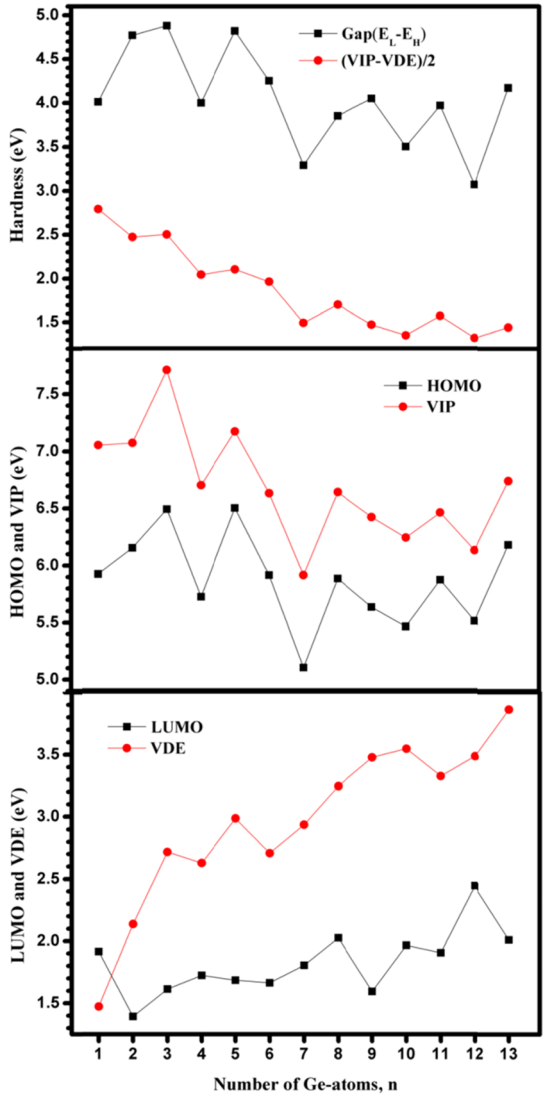

Figure 11. Chemical hardness and HOMO-LUMO gap of $AgGe_n$ clusters.

same as those in neutral clusters, revealing that the extra electron is completely localized in the germanium clusters. Ag atoms in cationic $AgGe_n^+$ (n = 1−12) clusters also act as electron donors. The charges of Ag atoms in cationic $AgGe_n^+$ (n = 1−12) clusters are 0.20−0.69 a.u. which are larger by 0.14−0.47 a.u. as compared with the charges of Ag atoms in neutral clusters. That is to say the germanium clusters provide the majority of lost charges for cationic $AgGe_n^+$ (n = 1−12) species. The charges of Ag atoms in the cage-like configuration of $AgGe_{12}$, $AgGe_{12}^-$, and $AgGe_{13}^+$ clusters are by −1.8 a.u., indicating that Ag atoms in these clusters act as an electron acceptor.

To better explore the electronic properties and HOMO-LUMO gap changes caused by the doping of Ag atoms, the detailed density of states (DOS) of $AgGe_7$ as an example is provided. The PDOS of pure Ge_7 and $AgGe_7$ is shown in Figure 12. It can be seen from Figure 12 that the position of

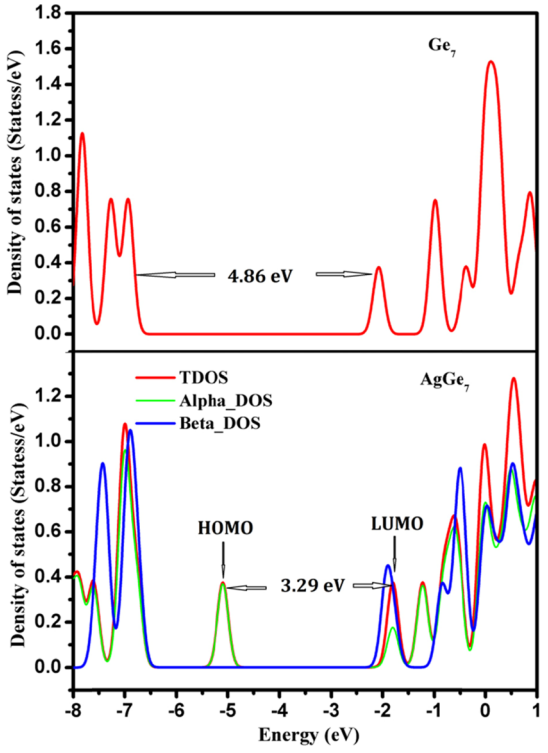

Figure 12. PDOSs for Ge_7 and $AgGe_7$ show a significant change in the PDOS at the Fermi level because of doping of Ag.

Table 5. Natural Population Analysis (NPA) Valence Configurations and Charge of Ag Atoms (in a.u.) Calculated with the mPW2PLYP Method for the Most Stable Structure $AgGe_n$ (n = 1−13) and Their Charged Clusters

species	charge	electron configuration	species	charge	electron configuration	species	charge	electron configuration
AgGe	−0.05	[core]$5s^{1.07}4d^{9.86}5p^{0.05}$	$AgGe^-$	−0.05	[core]$5s^{1.22}4d^{9.87}5p^{0.11}$	$AgGe^+$	0.20	[core]$5s^{0.84}4d^{9.85}5p^{0.05}$
$AgGe_2$	0.20	[core]$5s^{0.79}4d^{9.87}5p^{0.08}$	$AgGe_2^-$	0.20	[core]$5s^{0.84}4d^{9.87}5p^{0.19}$	$AgGe_2^+$	0.41	[core]$5s^{0.61}4d^{9.86}5p^{0.07}$
$AgGe_3$	0.28	[core]$5s^{0.70}4d^{9.86}5p^{0.11}$	$AgGe_3^-$	0.28	[core]$5s^{0.88}4d^{9.86}5p^{0.24}$	$AgGe_3^+$	0.45	[core]$5s^{0.56}4d^{9.86}5p^{0.07}$
$AgGe_4$	0.32	[core]$5s^{0.63}4d^{9.87}5p^{0.12}$	$AgGe_4^-$	0.32	[core]$5s^{1.06}4d^{9.88}5p^{0.09}$	$AgGe_4^+$	0.68	[core]$5s^{0.38}4d^{9.89}5p^{0.01}$
$AgGe_5$	0.28	[core]$5s^{0.59}4d^{9.86}5p^{0.22}$	$AgGe_5^-$	0.28	[core]$5s^{0.69}4d^{9.86}5p^{0.29}$	$AgGe_5^+$	0.42	[core]$5s^{0.50}4d^{9.85}5p^{0.18}$
$AgGe_6$	0.30	[core]$5s^{0.62}4d^{9.85}5p^{0.18}$	$AgGe_6^-$	0.30	[core]$5s^{0.73}4d^{9.83}5p^{0.38}$	$AgGe_6^+$	0.69	[core]$5s^{0.36}4d^{9.89}5p^{0.01}$
$AgGe_7$	0.48	[core]$5s^{0.49}4d^{9.88}5p^{0.11}$	$AgGe_7^-$	0.48	[core]$5s^{1.03}4d^{9.88}5p^{0.06}$	$AgGe_7^+$	0.64	[core]$5s^{0.37}4d^{9.88}5p^{0.07}$
$AgGe_8$	0.16	[core]$5s^{0.59}4d^{9.82}5p^{0.37}$	$AgGe_8^-$	0.16	[core]$5s^{0.62}4d^{9.81}5p^{0.67}$	$AgGe_8^+$	0.37	[core]$5s^{0.65}4d^{9.88}5p^{0.05}$
$AgGe_9$	0.19	[core]$5s^{0.60}4d^{9.84}5p^{0.31}$	$AgGe_9^-$	0.19	[core]$5s^{0.61}4d^{9.87}5p^{0.22}$	$AgGe_9^+$	0.63	[core]$5s^{0.40}4d^{9.87}5p^{0.05}$
$AgGe_{10}$	0.32	[core]$5s^{0.63}4d^{9.86}5p^{0.14}$	$AgGe_{10}^-$	0.32	[core]$5s^{0.60}4d^{9.88}5p^{0.19}$	$AgGe_{10}^+$	0.58	[core]$5s^{0.40}4d^{9.88}5p^{0.09}$
$AgGe_{11}$	0.02	[core]$5s^{0.56}4d^{9.82}5p^{0.53}$	$AgGe_{11}^-$	0.02	[core]$5s^{0.63}4d^{9.81}5p^{0.74}$	$AgGe_{11}^+$	0.50	[core]$5s^{0.51}4d^{9.86}5p^{0.09}$
$AgGe_{12}$	−1.80	[core]$5s^{0.67}4d^{9.77}5p^{2.24}$	$AgGe_{12}^-$	−1.80	[core]$5s^{0.63}4d^{9.84}5p^{2.70}$	$AgGe_{12}^+$	0.53	[core]$5s^{0.46}4d^{9.87}5p^{0.09}$
$AgGe_{13}$	0.23	[core]$5s^{0.63}4d^{9.83}5p^{0.25}$	$AgGe_{13}^-$	0.23	[core]$5s^{0.70}4d^{9.84}5p^{0.25}$	$AgGe_{13}^+$	−1.78	[core]$5s^{0.68}4d^{9.78}5p^{2.21}$

https://doi.org/10.1021/acsomega.1c00501
ACS Omega 2021, 6, 9813−9827

occupied spin up and spin down states is identical for DOS of pure Ge_7. However, after the doping of Ag atoms, a new occupied spin up state in DOS is created, which causes a significant change in the HOMO-LUMO gap (from 4.86 to 3.29 eV). The electronic states of the HOMO mainly come from the 5*s* orbital of Ag atoms and 4*s* and 4*p* orbitals of the Ge_7 cluster because the 0.48 a.u. charge transfer from the 5*s* orbital of Ag atoms to the 4*s*4*p* orbital of the Ge_7 cluster as can be seen from Table 5.

4. CONCLUSIONS

A systematic investigation of the silver-doped germanium clusters $AgGe_n$ with n = 1−13 in the neutral, anionic, and cationic states is performed using the unbiased global search technique combined with the double-density functional scheme. The lowest-energy minima of the clusters are identified based on calculated energies and the measured PES. Total atomization energies and thermochemical properties such as EA, IP, binding energy, hardness, and HOMO-LUMO gap are obtained and compared with those of pure germanium clusters. The structural evolution for $AgGe_n^{\lambda}$ (n = 1−13; λ = −1, 0, and +1) emerges as follows: For neutral and anionic clusters, although the most stable structures are inconsistent when n = 7−10, the structure patterns both are exohedral structures except for n = 12, and a highly symmetrical endohedral configuration is formed when n = 12. For the cationic state, the most stable structures are attaching structures (in which an Ag atom is adsorbed on the Ge_n cluster or a Ge atom is adsorbed on the $AgGe_{n-1}$ cluster) at n = 1−12, and when n = 13, the cage configuration is formed. The analyses of binding energy indicate that doping of an Ag atom into the neutral and charged Ge_n clusters may decrease their stability. The EAs of $AgGe_n$ clusters including AEAs and VDEs are presented and are in perfect agreement with the experimental values. The IP including VIP and AIP of neutral Ge_n clusters is decreased when doped with an Ag atom. The HOMO-LUMO gaps of neutral $AgGe_n$ (n = 1−13) excluded n = 8 and 12 are larger than that of anionic clusters. For cationic states, the HOMO-LUMO gaps of $AgGe_n^+$ are wider than that of $AgGe_n$ for n = 1, 2, 4, and 6−10 and are narrower for n = 3, 5, and 11−13. The variant trend of the HOMO-LUMO gap and hardness versus cluster size is slightly different. The accuracy of the theoretical analyses in this paper is demonstrated successfully by the agreement between simulated and experimental results such as PES, IP, EA, and binding energy.

AUTHOR INFORMATION

Corresponding Author

Jucai Yang − *School of Chemical Engineering, Inner Mongolia Key Laboratory of Theoretical and Computational Chemistry Simulation and School of Energy and Power Engineering, Inner Mongolia University of Technology, Hohhot 010051, People's Republic of China;* orcid.org/0000-0003-4998-0364; Email: yangjc@imut.edu.cn

Author

Bin Liu − *School of Chemical Engineering, Inner Mongolia Key Laboratory of Theoretical and Computational Chemistry Simulation, Inner Mongolia University of Technology, Hohhot 010051, People's Republic of China*

Complete contact information is available at: https://pubs.acs.org/10.1021/acsomega.1c00501

Notes

The authors declare no competing financial interest.

ACKNOWLEDGMENTS

This study was supported by the National Natural Science Foundation of China (Grant No. 21863007) and by the Science and Technology Plan Project in Inner Mongolia Autonomous Region (Grant No. JH20180633).

REFERENCES

(1) Ravi, P. Academic and Industry Research Progress in Germanium Nanodevices. *Nature* **2011**, *479*, 324−328.

(2) Truong, B. T.; Minh, T. N. A Stochastic Search for the Structures of Small Germanium Clusters and Their Anions: Enhanced Stability by Spherical Aromaticity of the Ge_{10} and Ge_{12}^{2-} systems. *J. Chem. Theory Comput.* **2011**, *7*, 11190−11130.

(3) Bulusu, S.; Yoo, S.; Zeng, X. C. Search for Global Minimum Geometries for Medium Sized Germanium Clusters: Ge_{12}-Ge_{20}. *J. Chem. Phys.* **2005**, *122*, 164305.

(4) Wei, A. Predicting the Structural Evolution of Ge_n^- ($3 \le n \le 20$) Clusters: an Anion Photoelectron Spectroscopy Simulation. *Phys. Chem. Chem. Phys.* **2018**, *20*, 25746−25751.

(5) Yoshida, S.; Fuke, K. Photoionization Studies of Germanium and Tin Clusters in the Energy Region of 5.0-8.8 eV: Ionization Potentials for Ge_n (n=2-57) and Sn_n(n=2-41). *J. Chem. Phys.* **1999**, *111*, 3880−3890.

(6) Gingerich, K. A.; Schmude, R. W., Jr.; Baba, M. S.; Meloni, G. Atomization Enthalpies and Enthalpies of Formation of the Germanium Clusters, Ge_5, Ge_6, Ge_7, and Ge_8 by Knudsen Effusion Mass Spectrometry. *J. Chem. Phys.* **2000**, *112*, 7443−7448.

(7) Gingerich, K. A.; Baba, M. S.; Schmude, R. W., Jr.; Kingcade, J. E., Jr. Atomization Enthalpies and Enthalpies of Formation of Ge_3 and Ge_4 by Knudsen Effusion Mass Spectrometry. *Chem. Phys.* **2000**, *262*, 65−74.

(8) Hunter, J. M.; Fye, J. L.; Jarrold, M. F.; Bower, J. E. Structural Transitions in Size-selected Germanium Cluster Ions. *Phys. Rev. Lett.* **1994**, *73*, 2063−2066.

(9) Li, S. D.; Zhao, Z. G.; Wu, H. S.; Jin, Z. H. Ionization Potentials, Electron Affinities, and Vibrational Frequencies of Ge_n (n=5-10) Neutrals and Charged Ions from Density Functional Theory. *J. Chem. Phys.* **2001**, *115*, 9255−9259.

(10) Negishi, Y.; Kawamata, H.; Hayakawa, F.; Nakajima, A.; Kaya, K. The Infrared HOMO-LUMO Gap of Germanium Clusters. *Chem. Phys. Lett.* **1998**, *294*, 370−376.

(11) Negishi, Y.; Kawamata, H.; Hayase, T.; Gomei, M.; Kishi, R.; Hayakawa, F.; Nakajima, A.; Kaya, K. Photoelectron Spectroscopy of Germanium-Fluorine Binary Clusteranions: the HOMO-LUMO Gap Estimation of Ge_n Clusters. *Chem. Phys. Lett.* **1997**, *269*, 199−207.

(12) Burton, G. R.; Xu, C.; Arnold, C. C.; Neumark, D. M. Photoelectron Spectroscopy and Zero Electron Kinetic Energy Spectroscopy of Germanium Cluster Anions. *J. Chem. Phys.* **1996**, *104*, 2757−2764.

(13) Kingcade, J. E.; Nagarathna-Naik, H. M.; Shim, I.; Gingerich, K. A. Electronic Structure and Bonding of the Molecule Ge_2 from All-Electron ab Initio Calculations and Equilibrium Measurements. *Phys. Chem.* **1986**, *90*, 2830−2834.

(14) Arthur, K.; Bernard, H. S. Atomization Energies of the Polymers of Germanium, Ge_2 to Ge_7. *J. Chem. Phys.* **1966**, *45*, 822−826.

(15) Hostutler, D. A.; Li, H. Y.; Clouthier, D. J.; Wannous, G. Exploring the Bermuda Triangle of Homonuclear Diatomic Spectroscopy: The Electronic Spectrum and Structure of Ge_2. *J. Chem. Phys.* **2002**, *116*, 4135−4141.

(16) Zhao, J.; Du, Q.; Zhou, S.; Kumar, V. Endohedrally Doped Cage Clusters. *Chem. Rev.* **2020**, *120*, 9021−9163.

(17) Siouani, C.; Mahtout, S.; Rabiloud, F. Structure, Stability, and Electronic Properties of Niobium-Germanium and Tantalum-Germanium Clusters. *J. Mol. Model.* **2019**, *25*, 113.

(18) Lasmi, M.; Mahtout, S.; Rabilloud, F. The Effect of Palladium and Platinum Doping on the Structure, Stability and Optical Properties of Germanium Clusters: DFT Study of $PdGe_n$ and $PtGe_n$ (n=1-20) Clusters. *Comput. Theor. Chem.* **2020**, *1181*, 112830.
(19) Mahtout, S.; Siouani, C.; Rabilloud, F. Growth Behavior and Electronic Structure of Noble Metal-Doped Germanium Clusters. *J. Phys. Chem. A* **2018**, *122*, 662−677.
(20) Siouani, C.; Mahtout, S.; Safer, S.; Rabilloud, F. Structure, Stability, and Electronic and Magnetic Properties of VGe_n(n = 1−19) Clusters. *J. Phys. Chem. A* **2017**, *121*, 3540−3554.
(21) Atobe, J.; Koyasu, K.; Furusea, S.; Nakajima, A. Anion Photoelectron Spectroscopy of Germanium and Tin Clusters Containing a Transition- or Lanthanide-Metal Atom; MGe_n^- (n= 8-20) and MSn_n^- (n=15-17) (M = Sc-V, Y-Nb, and Lu-Ta). *Phys. Chem. Chem. Phys.* **2012**, *14*, 9403−9410.
(22) Xiang, Y. K. *The Electronic Structures and Properties of Transition Metal Doped Si, Ge Clusters and Ag-BO2 clusters.* Ph.D. Dissertation, Institute of Chemistry, University of Chinese Academy of Sciences, 2014.
(23) Deng, X. J.; Kong, X. Y.; Xu, X. L.; Xu, H. G.; Feng, X. G.; Zheng, W. J. Photoelectron Spectroscopy and Density Functional Calculations of VGe_n^- (n=3-12) Clusters. *J. Phys. Chem. C* **2015**, *119*, 11048−11055.
(24) Deng, X. J.; Kong, X. Y.; Xu, X. L.; Xu, H. G.; Zheng, W. J. Structural and Magnetic Properties of $CoGe_n^-$ (n=2-11) Clusters: Photoelectron Spectroscopy and Density Functional Calculations. *Chem. Phys. Chem.* **2014**, *15*, 3987−3993.
(25) Deng, X. J.; Kong, X. Y.; Xu, H. G.; Feng, X. G.; Zheng, W. J. Structural and Magnetic Properties of $FeGe_n^{-/0}$ (n=3-12) Clusters: Mass-Selected Anion Photoelectron Spectroscopy and Density Functional Theory Calculations. *J. Chem. Phys.* **2017**, *147*, 234310.
(26) Lu, S. J.; Hu, L. R.; Xu, X. L.; Xu, H. G.; Chen, H.; Zheng, W. J. Transition from Exohedral to Endohedral Structures of $AuGe_n^-$ (n=2-12) Clusters: Photoelectron Spectroscopy and ab initio Calculations. *Phys. Chem. Chem. Phys.* **2016**, *18*, 20321−20329.
(27) Deng, X. J.; Kong, X. Y.; Xu, X. L.; Xu, H. G.; Zheng, W. J. Photoelectron Spectroscopy and Density Functional Calculations of $TiGe_n^-$ (n=7-12) Clusters. *Chin. J. Chem. Phys.* **2016**, *29*, 123−128.
(28) Deng, X. J.; Kong, X. Y.; Xu, X. L.; Xu, H. G.; Zheng, W. J. Structural and Bonding Properties of Small $TiGe_n^-$ (n=2-6) Clusters: Photoelectron Spectroscopy and Density Functional Calculations. *RSC Adv.* **2014**, *4*, 25963−25968.
(29) Lu, S. J.; Farooq, U.; Xu, H. G.; Xu, X. L.; Zheng, W. J. Structural Evolution and Electronic Properties of $Au_2Ge_n^{-1/0}$ (n=1-8) Clusters: Anion Photoelectron Spectroscopy and Theoretical Calculations. *Chin. J. Chem. Phys.* **2019**, *32*, 229−240.
(30) Liang, X. Q.; Deng, X. J.; Lu, S. J.; Huang, X. M.; Zhao, J. J.; Xu, H. G.; Zheng, W. J. Probing Structural, Electronic, and Magnetic Properties of Iron-Doped Semiconductor Clusters $Fe_2Ge_n^{-/0}$ (n=3-12) via Joint Photoelectron Spectroscopy and Density Functional Study. *J. Phys. Chem. C* **2017**, *121*, 7037−7046.
(31) Liang, X. Q.; Kong, X. Y.; Lu, S. J.; Huang, X. M.; Zhao, J. J.; Xu, H. G.; Zheng, W. J. Structural Evolution and Magnetic Properties of Anionic Clusters Cr_2Ge_n (n=3-14): Pphotoelectron Spectroscopy and Density Functional Theory Computation. *J. Phys.: Condens. Matter* **2018**, *30*, 335501.
(32) Pham, L. N.; Nguyen, M. T. Titanium Digermanium: Theoretical Assignment of Electronic Transitions Underlying its Anion Photoelectron Spectrum. *J. Phys. Chem. A* **2017**, *121*, 1940−1949.
(33) Pham, L. N.; Nguyen, M. T. Insights into Geometric and Electronic Structures of $VGe_3^{-/0}$ Clusters from Anion Photoelectron Spectrum Assignment. *J. Phys. Chem. A* **2017**, *121*, 6949−6956.
(34) Hou, X. J.; Gopakumar, G.; Lievens, P.; Nguyen, M. T. Chromium-Doped Germanium Clusters $CrGe_n$ (n=1-5): Geometry, Electronic Structure, and Topology of Chemical Bonding. *J. Phys. Chem. A* **2007**, *111*, 13544−13553.
(35) Tran, V. T.; Tran, Q. T. Electronic Structures of $NbGe_n^{-/0/+}$ (n=1-3) Clusters from Multiconfigurational CASPT2 and Density Matrix Renormalization Group-CASPT2 Calculations. *J. Comput. Chem.* **2020**, *41*, 2641−2652.
(36) Tran, V. T.; Tran, Q. T. Spin State Energetics of $VGe_n^{-/0}$ (n=5-7) Clusters and New Assignments of the Anion photoelectron Spectra. *J. Comput. Chem.* **2018**, *39*, 2103−2109.
(37) Wang, J. G.; Ma, L.; Zhao, J. J.; Wang, G. H. Structural Growth Sequences and Electronic Properties of Manganese-Doped Germanium Clusters: $MnGe_n$ (2-15). *J. Phys.: Condens. Matter* **2008**, *20*, 335223.
(38) Kapila, N.; Garg, I.; Jindal, V. K.; Sharma, H. First Principle Investigation into Structural Growth and Magnetic Properties in Ge_nCr Clusters for n=1-13. *J. Magn. Mater.* **2012**, *324*, 2885−2893.
(39) Trivedi, R.; Dhaka, K.; Bandyopadhyay, D. Study of Electronic Properties, Stabilities and Magnetic Quenching of Molybdenum-Doped Germanium Clusters: a Density Functional Investigation. *RSC Adv.* **2014**, *4*, 64825−64834.
(40) Triedi, R. K.; Bandyopadhyay, D. Insights of the Role of Shell Closing Model and NICS in the Stability of $NbGe_n$ (n=7-18) Clusters: a First Principles Investigation. *J. Mater. Sci.* **2019**, *54*, 515−528.
(41) Bandyopadhyay, D.; Sen, P. Density Functional Investigation of Structure and Stability of Ge_n and Ge_nNi (n=1-20) Clusters: Validity of the Electron Counting Rule. *J. Phys. Chem. A* **2010**, *114*, 1835−1842.
(42) Bandyopadhyay, D.; Kaur, P.; Sen, P. New Insights into Applicability of Electron-Counting Rules in Transition Metal Encapsulating Ge Cage Clusters. *J. Phys. Chem. A* **2010**, *114*, 12986−12991.
(43) Kumar, M.; Bhattacharyya, N.; Bandyopadhyay, D. Architecture, Electronic Structure and Stability of TM@Ge(n) (TM=Ti, Zr and Hf; n=1-20) Clusters: a Density Functional Modeling. *J. Mol. Model.* **2012**, *18*, 405−418.
(44) Bandyopadhyay, D. Architectures, Electronic Structures, and Stabilities of Cu-Doped Ge_n Clusters: Density Functional Modeling. *J. Mol. Model.* **2012**, *18*, 3887−3902.
(45) Bandyopadhyay, D. Electronic Structure and Stability of Anionic $AuGe_n$ (n=1-20) Clusters and Assemblies: A Density Functional Modeling. *Struct. Chem.* **2019**, *30*, 955−963.
(46) Borshch, N. A.; Pereslavtseva, N. S.; Kurganskii, S. I. Spatial Structure and Electron Energy Spectra of $ScGe_n^-$ (n=6-16) Clusters. *Russ. J. Phys. Chem. B* **2015**, *9*, 9−18.
(47) Borshch, N. A.; Kurganskii, S. I. Atomic Structure and Electronic Properties of Anionic Germanium-Zirconium Clusters. *Inorg. Mater.* **2018**, *54*, 1−7.
(48) Borshch, N. A.; Kurganskii, S. I. Spatial Structure and Electron Energy Spectrum of $HfGe_n^-$ (n=6-20) Clusters. *Inorg. Mater.* **2015**, *51*, 870−876.
(49) Borshch, N. A.; Kurganskii, S. I. Anionic Germanium-Niobium Clusters: Atomic Structure, Mechanisms of Cluster Formation, and Electronic Spectra. *Russ. J. Phys. Chem. A* **2018**, *92*, 1720−1726.
(50) Borshch, N. A.; Pereslavtseva, N. S.; Kurganskii, S. I. Spatial and Electronic Structures of the Germanium-Tantalum Clusters $TaGe_n^-$ (n=8-17). *Phys. Solid. State* **2014**, *56*, 2336−2342.
(51) Jaiswal, S.; Kumar, V. Growth Behavior and Electronic Structure of Neutral and Anion $ZrGe_n$(n=1-21) Clusters. *Comput. Theor. Chem.* **2016**, *1075*, 87−97.
(52) Trivedi, R.; Bandyopadhyay, D. Evolution of Electronic and Vibrational Properties of $M@X_n$ (M=Ag, Au, X=Ge, Si, n=10, 12, 14) Clusters: a Density Functional Modeling. *J. Mater. Sci.* **2018**, *53*, 8263−8273.
(53) Trivedi, R.; Mishra, V. Exploring the Structural Stability Order and Electronic Properties of Transition Metal M@Ge12 (M=Co, Pd, Tc, and Zr) Doped Germanium cage clusters − A Density Functional Simulation. *J. Mol. Struct.* **2021**, *1226*, No. 129371.
(54) Qin, W.; Lu, W. C.; Xia, L. H.; Zhao, L. Z.; Zang, Q. J.; Wang, C. Z.; Ho, K. M. Structures and Stability of Metal-Doped Ge_nM (n=9, 10) Clusters. *AIP. Adv.* **2015**, *5*, No. 067159.

https://doi.org/10.1021/acsomega.1c00501
ACS Omega 2021, 6, 9813−9827

(55) Zhang, J.; Dolg, M. ABCluster: the Artificial Bee Colony Algorithm for Cluster Global Optimization. *Phys. Chem. Chem. Phys.* **2015**, *17*, 24173−24181.
(56) Zhang, J.; Dolg, M. Global Optimization of Clusters of Rigid Molecules Using the Artificial Bee Colony Algorithm. *Phys. Chem. Chem. Phys.* **2016**, *18*, 3003−3010.
(57) Zhang, J.; Glezakou, V. A.; Rousseau, R.; Nguyen, M. T. NWPEsSe: an Adaptive-Learning Global Optimization Algorithm for Nanosized Cluster Systems. *J. Chem. Theory Comput.* **2020**, *16*, 3947−3958.
(58) Frisch, M. J.; Trucks, G. W.; Schlegel, H. B.; Scuseria, G. E.; Robb, M. A.; Cheeseman, J. R.; Scalmani, G.; Barone, V.; Mennucci, B.; Petersson, G. A.; Nakatsuji, H.; et al. *Gaussian 09, Revision C.01*,Gaussian, Inc.: Wallingford CT, 2010.
(59) Adamo, C.; Barone, V. Toward Reliable Density Functional Methods without Adjustable Parameters: The PBE0 Model. *J. Chem. Phys.* **1999**, *110*, 6158−6170.
(60) Hay, P. J.; Wadt, W. R. Ab Initio Effective Core Potentials for Molecular Calculations. Potentials for the Transition Metal Atoms Sc to Hg. *J. Chem. Phys.* **1985**, *82*, 270−283.
(61) Peterson, K. A.; Puzzarini, C. Systematically Convergent Basis Sets for Transition Metals. II. Pseudopotential-Based Correlation Consistent Basis Sets for the Group 11 (Cu, Ag, Au) and 12 (Zn, Cd, Hg) Elements. *Theor. Chem. Acc.* **2005**, *114*, 283−296.
(62) Peterson, K. A. Systematically Convergent Basis Sets with Relativistic Pseudopotentials. I. Correlation Consistent Basis Sets for the Post-d Group 13-15 Elements. *J. Chem. Phys.* **2003**, *119*, 11099−11112.
(63) Schwabe, T.; Grimme, S. Towards Chemical Accuracy for the Thermodynamics of Large Molecules: New Hybrid Density Functionals Including Non-local Correlation Effects. *Phys. Chem. Chem. Phys.* **2006**, *8*, 4398−4401.
(64) Wilson, A. K.; Woon, D. E.; Peterson, K. A.; Dunning, T. H., Jr. Gaussian Basis Sets for Use in Correlated Molecular Calculations. IX. The Atom Gallium through Krypton. *J. Chem. Phys.* **1999**, *110*, 7667−7676.
(65) Liu, Y.; Yang, J.; Cheng, L. Structural Stability and Evolution of Scandium-Doped Silicon Clusters: Evolution of Linked to Encapsulated Structures and Its Influence on the Prediction of Electron Affinities for $ScSi_n$(n=4-16) Clusters. *Inorg. Chem.* **2018**, *57*, 12934−12940.
(66) Neckel, A.; Sodeek, G. Bestimmung Der Dissoziationsenergien Der Gasformigen Molekule CuGe, AgGe and AuGe. *Monatsh. Chem.* **1972**, *103*, 367−382.
(67) Liu, B.; Wang, X.; Yang, J. Comparative Research of Configuration, Stability and Electronic Properties of Cationic and Neutral $[AuGe_n]^{\lambda}$ and $[Ge_{n+1}]^{\lambda}$ (n=1-13, λ=0,+1). *Mater. Today. Commun.* **2021**, *26*, No. 101989.
(68) Lu, T.; Chen, F. Multiwfn: A Multifunctional Wavefunction Analyzer. *J. Comput. Chem.* **2012**, *33*, 580−592.

https://doi.org/10.1021/acsomega.1c00501
ACS Omega 2021, 6, 9813−9827